Assessment of Short-medium Term Intervention Effects Using CAESAR-Lisflood in Post-earthquake Mountainous Area

Di Wang[1,2,3], Ming Wang[1], Kai Liu[1]

[1]School of National Safety and Emergency Management, Beijing Normal University, Beijing, China.

[2]Academy of Disaster Reduction and Emergency Management, Beijing Normal University, Beijing, China.

[3]Faculty of Geographical Science, Beijing Normal University, Beijing, China.

Correspondence to: Ming Wang (wangming@bnu.edu.cn)

Abstract

. The 2008 Wenchuan earthquake triggered local geomorphic changes rapidly and gradually ~~and produced~~, producing abundant materials through external processes. The ~~abundant~~substantial materials increased the risks of geomorphic hazards (flash floods, landslides, and debris flows) induced by extreme precipitation in the area. ~~To reduce sediment transport present in geomorphic hazards, intervention~~Intervention measures such as dams, levees, and vegetation revetments have been constructed in specified sites to reduce sediment transport.

This study concentrated on ~~the assessment of~~assessing intervention effects incorporated with various facilities on post-earthquake fragile mountains in the short-medium term. ~~Take~~Taking the Xingping valley as an example, we used the CAESAR-Lisflood landscape evolution model to simulate three ~~different~~ scenarios ~~including~~: unprotected landscapes, present protected landscapes, and enhanced protected landscapes ~~in~~between 2011- and 2013. We compared the geomorphic changes and defined two indicators to assess the intervention effects.

The results showed that the mitigation facilities were effective, especially engineering ~~measures that cooperated~~efforts cooperating with vegetation revetments in the upstream area~~,~~. The distribution patterns of erosion and ~~the present mitigation measures were inadequate to stop materials loss and prevent hazards from the upstream area. Moreover~~deposition changed considerably by the intervention measures. Additionally, the effectiveness ~~reduced gradually~~of each intervention scenario showed a gradual decline caused directly by the ~~storage~~reduction of the reservoir capacity ~~of dams decreased~~. Besides, the enhanced scenario functioned better than the present one with a smaller descent slope. The simulation methods assessed the ability and effectiveness of cooperated control measures and could support optimum mitigation strategies.

1~~.~~ Introduction

~~Strong earthquake shaking fractures rock mass; the resulting cracks are propagated into a weak plane (Huang, 2009) by weathering and erosion; the resulting source materials increase in mountainous regions, and modify mountain landscapes by various surface processes for days, years, and millennia (Fan et al., 2019). That means the quake-stricken areas will trigger landslides (a general term to describe the downslope movement of soil, rock, and organic materials under the influence of gravity and also the landform that results from such movement) by complicated processes. The devastating earthquake measuring Ms =8.0 (the surface-wave magnitude which is the logarithm of the maximum amplitude of ground motion for surface waves with a wave period of 20 seconds) that struck the Wenchuan area has produced landslides that threaten highways,~~

样式定义：正文：字体：（中文）宋体，10 磅，两端对齐，缩进：首行缩进： 0 厘米，行距：1.5 倍行距

样式定义：标题 1：字体：10 磅，两端对齐，缩进：左侧： 0 厘米，首行缩进： 0 厘米，段落间距段前：24 磅，段后：12 磅，行距：单倍行距

样式定义：标题 2：字体：10 磅，加粗，非倾斜，两端对齐，缩进：左侧： 0 厘米，首行缩进： 0 厘米，段落间距段前：12 磅，段后：12 磅，行距：单倍行距

样式定义：标题 3：字体：（中文）宋体，10 磅，两端对齐，缩进：首行缩进： 0 厘米，段落间距段前：12 磅，段后：12 磅，行距：单倍行距

样式定义：图片表格：字体：10 磅，两端对齐，行距：1.5 倍行距

样式定义：题注：两端对齐，缩进：首行缩进： 0 厘米，行距：1.5 倍行距

设置了格式：字体：17 磅

带格式的：左侧： 1.65 厘米，右侧： 1.65 厘米，顶端： 1 厘米，底端： 2.36 厘米

带格式的：左，缩进：左侧： 0 厘米，首行缩进： 0 字符，段落间距段前：18 磅，行距：固定值 22 磅

设置了格式：字体：12 磅

带格式的：段落间距段前：9 磅

设置了格式：字体：12 磅

设置了格式：字体：（中文）Times New Roman，12 磅

带格式的：段落间距段前：6 磅

设置了格式：字体颜色：自动设置

带格式的：摘要，段落间距段前：6 磅，段后：18 磅

带格式的：摘要，缩进：左侧： 0 厘米，首行缩进： 0 厘米，右侧： 0 厘米，行距：单倍行距

设置了格式：下划线

设置了格式：字体：Times New Roman，加粗

带格式的：段落间距段后：0 磅，行距：单倍行距

设置了格式：字体：Times New Roman

railways, towns, and other infrastructure. Although limited comprehensive mitigation measures were constructed in potentially dangerous sites, disasters still occurred because of complex processes and origins, high-frequency precipitation, and the low cost of treatment (Cui et al., 2013; Yu et al., 2010). Therefore, understanding intervention measures is crucial for effective mitigation. More studies mainly focus on the establishment of post-evaluation effectiveness index systems without more practices (N. Wang et al., 2015; L. Zhang and Liang, 2005) and long-term measurement of changes before and after mitigation measurement by field surveys (Chen et al., 2013; Zhou et al., 2012). The subjective expression determines that the index system establishment is still in the theoretical stage and the measurement cost is high in time and money. Recent research compares the disaster characteristics before and after the intervention, which are quickly obtained from disaster simulation (Cong et al., 2019). While the characteristics express the process ignoring the long time effects on the geomorphic changes. Thus, the short-medium term and spatial geomorphic changes quickly obtained from the simulation will provide more details to interpret engineering measures in special sites even in those inaccessible to humans.

The open access 2-D landscape evolution model CAESAR-Lisflood (C-L) is based on Cell Automata (CA) framework, which has powerful spatial modeling and computing capabilities to simulate complex dynamic systems (Batty et al., 1997; Batty and Xie, 1997; Couclelis, 1997), enables the study of many earth system interactions with different environmental forces. Representation of deposition and erosion within C-L is used widely in rehabilitation planning and soil erosion predictions from a post-mining landform (Hancock et al., 2017; J.B.C.Lowry et al., 2019; Saynor et al., 2019; Slingerland et al., 2019; Thomson and Chandler, 2019) and channel evolution and sedimentary budget in dam settings (Gioia and Schiattarella, 2020; Poeppl et al., 2019). In addition, there have been a series of studies in the mountainous area involving secondary geo-hazard driving factors (Li et al., 2018; M. Wang, Liu, et al., 2014) and vegetation recovery (X. Zhang et al., 2018). C-L was used with different scenarios of rainfall or future climate change to interpret the landscape evolution after the Wenchuan earthquake (Li et al., 2020; Xie et al., 2018). The methods and parameters values used in the above research helped to promote the application in other study areas.

In this study, we compared the short-medium term scenario simulations toStrong earthquakes trigger co-seismic landslides and crack the mountains discontinuously, increasing weak structural planes (Huang, 2009) by weathering and erosion. Consequently, the source materials produced from co-seismic landslides and attendant mass failure caused by the weak slope increase in mountainous regions and modify mountain landscapes by various surface processes for days, years, and millennia (Fan et al., 2020). The Wenchuan 2008 Ms = 8.0 (the surface-wave magnitude, which is the logarithm of the maximum amplitude of ground motion for surface waves with a wave period of 20 seconds) earthquake influences towns and other infrastructure in the affected area. Many studies have mapped the landslides triggered by the devastating earthquake. Gorum et al. (2011) performed an extensive landslide interpretation using a large set of high-resolution optical images and mapped nearly 60000 individual landslides, which are no less than 600m^2. Xu et al. (2014) delineated 197481 landslides formed by polygons, centroids, and top points compiled from visual image interpretation. To estimate the threat of loose materials in subsequent sediment disasters caused by landslides, some research attempt to measure the volume of deposited materials based on field survey and assumptions. Huang and Fan (2013) estimated 400 million m^3 of materials deposited in the heavy-affected areas by assuming that the materials deposited on steep slopes with angles larger than 30° and a catchment area more extensive than 0.1 km^2. An approximate 2793 million m^3 of sediment was calculated by Chen et al. (2009) using different deposited depth settings in different buffer zones of the fault. In summary, a tremendous number of loose materials are suspended on the gullies and hill slopes and ready to be eroded and transported away over a long time. Therefore, the mitigation is still in the long run in the Wenchuan quake-stricken area.

Structural mitigation measures have been developed in the affected areas regarding the site conditions and technical and economic feasibilities. For example, Ecological mitigation such as vegetation revetments was conducted to stabilize the source area in hillslopes (Cui and Lin, 2013; Forbes and Broadhead, 2013; Stokes et al., 2014), and check dams were used widely to intercept upriver sediment (Yang et al., 2021; Marchi et al., 2019). Lateral walls and levees were the longitude structures (Marchi et al., 2019) to protect the infrastructures in mountain watersheds with higher sediment supply to the main streams.

Although comprehensive mitigation measures were performed in potentially dangerous sites, disasters still occurred owing to rough terrain, vague source materials, intensive precipitation, and relatively low-cost mitigating measures (Yu et al., 2010; Cui et al., 2013). Therefore, understanding the effectiveness of intervention measures is crucial for mitigation strategies. More studies mainly focus on establishing post-evaluation effectiveness index systems that are not supported by sufficient practices (Zhang and Liang, 2005; Wang et al., 2015). Other research on long-term on-site measurement required more energy and financing and compared the changes before and after the intervention measures (Zhou et al., 2012; Chen et al., 2013). Recent research compares the disaster characteristics before and after the intervention, which are quickly obtained from the simulation (Cong et al., 2019; He et al., 2022). Nevertheless, the characteristics express the process ignoring the long-time effects on the geomorphic changes (longer than the duration of a single event). Therefore, the short-medium term (from the duration to decades) and spatial geomorphic changes quickly obtained from the simulation will provide more details to interpret engineering measures in notable locations, even in those inaccessible to humans.

The open access 2-D landscape evolution model CAESAR-Lisflood (C-L) is based on the Cellular Automata (CA) framework (Coulthard et al., 2013), which has powerful spatial modelling and computing capabilities to simulate complex dynamic systems(Batty and Xie, 1997; Couclelis, 1997; Coulthard et al., 2002). The model enables the study of many earth system interactions with different environmental forces. Representation of deposition and erosion within C-L is used widely in rehabilitation planning and soil erosion predictions from a post-mining landform (Saynor et al., 2019; Hancock et al., 2017; J.B.C.Lowry et al., 2019; Thomson and Chandler, 2019; Slingerland et al., 2019) and channel evolution and sedimentary budget with dam settings (Poeppl et al., 2019; Gioia and Schiattarella, 2020; Ramirez et al., 2020, 2022). In addition, there have been a series of studies in the mountainous area involving secondary geo-hazard driving factors (Li et al., 2018; Wang et al., 2014b) and vegetation recovery (Zhang et al., 2018). Li et al. (2020) and Xie et al. (2018) have used C-L with different rainfall scenarios or future climate change to interpret the landscape evolution after the Wenchuan earthquake. The methods and parameter values used in the above research helped to promote the application in other study areas.

In this study, we simulated and compared the geomorphic changes and sediment output in three scenarios that varied in mitigation compositions and intensities in a catchment. The objectives are to 1) assess the effectiveness of a set of mitigation facilities ~~and to analyze~~in reducing sediment transport, 2) analyse the role of each ~~measure in the specific site. The results will guide the control of secondary geological disasters after an earthquake.~~ facility in geomorphic changes, and 3) determine vegetation influence on catchment erosion.

2~~.~~ Study area

2.1 Regional characteristics

The study area was Xingping valley in the northeastern Sichuan province, a left branch of the Shikan ~~River~~river (a tributary of the Fu River) ~~(Fig. 1).~~(Figure 1). There are nearly two hundred households scattered among more than five villages in the catchment. The topography of the catchment is rugged, with an elevation between 800 and 3036 m and an area of approximately 14 km^2. The catchment shape looks like a ~~“~~"leaf~~”~~" with a nearly U-shaped main ditch ~~characterized~~characterised by a

带格式的: 缩进: 左侧: 0 厘米, 首行缩进: 0 厘米, 右侧: 0 厘米, 行距: 单倍行距

设置了格式: 字体: (中文) 宋体, 突出显示

设置了格式: 字体: Times New Roman, 加粗

带格式的: 缩进: 左侧: 0 厘米, 行距: 单倍行距

设置了格式: 字体: Times New Roman

设置了格式: 字体: Times New Roman, 10 磅

设置了格式: 字体: Times New Roman

带格式的: 行距: 单倍行距, 制表位: 不在 10.08 字符

带格式的: 缩进: 左侧: 0 厘米, 首行缩进: 0 厘米, 右侧: 0 厘米, 段落间距段后: 0 磅, 行距: 单倍行距

high longitudinal gradient (~ 120‰) and more than ten small V-shaped branch gullies. The length from northeast to southwest is 5770 m, the other direction perpendicular to which is 4150 m. ~~The region is characterized by a~~A humid temperate climate with a mean annual temperature of 14.7℃~~.~~ characterises the region. The mean annual precipitation is ~~up to~~ 807.6 mm, with maxima daily rainfall between May and September. The steep terrain and short-term heavy rainfall make an ephemeral stream in this area.

~~The geological settings are mainly distributed metamorphic sandstones, sandy slate, crystalline limestone, and phyllite of Triassic Xikang Group (T_{3xk}) and Silurian Maoxian Group (S_{mx}), which easily induce a large amount of loose solid material after weathering of a static process. Wenchuan earthquake, a dynamic process made this area one of the most severely affected locations with a Modified Mercalli Intensity scale of IX and X (M. Wang, Yang, et al., 2014). The earthquake strengthened the solid material produced and reached 10^6 m^3 by triggering landslides and other surficial movements from Mayuanzi, Zhengjiashan, and Wujiaping (Fig. 1)(Guo et al., 2018).~~

The local basement rocks are mainly metamorphic sandstones, sandy slate, crystalline limestone, and phyllite of Triassic Xikang Group (T_{3xk}) and Silurian Maoxian Group (S_{mx}), which quickly induce a large amount of loose solid material after weathering of a static process. Consequently, the Wenchuan earthquake that made this area one of the most severely affected locations with a Modified Mercalli Intensity scale of X (Wang et al., 2014a) produced 10^6 m^3 by triggering landslides from Mayuanzi, Zhengjiashan, and Wujiaping (Figure 1)(Guo et al., 2018).

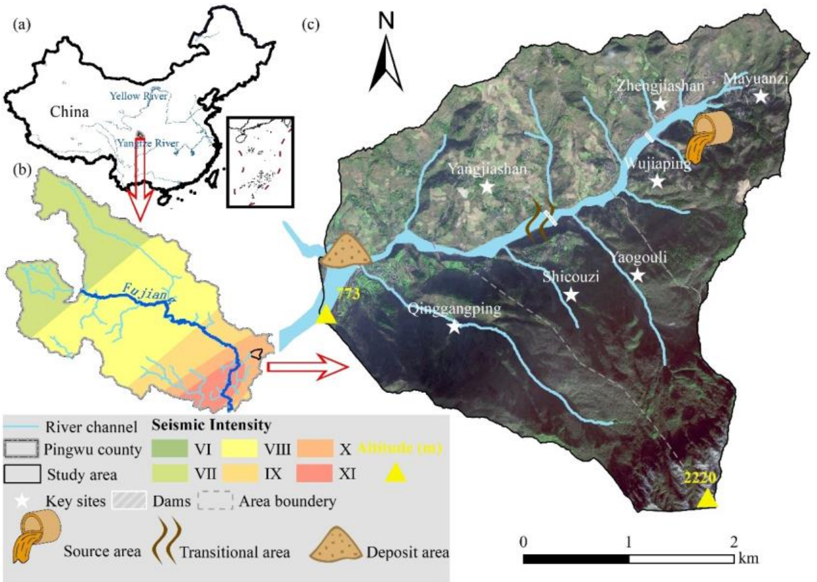

Figure 1: The location of the study area. (a) Location within China; (b) Location within the seismic intensity ranges of the Wenchuan earthquake and the Pingwu county; (c) The image of the area.

2.2 Historical hazards and intervention measures

~~To reflect most of the landslides processes in spatial relationships according to the site survey and literature research on the characteristics of the historical hazard, we divided the study area into three regions: source area, translation area, and deposit area (Feng et al., 2017; Guo et al., 2018; Zhao et al., 2019) (the dashed lines in Fig. 1. (c)). The loose solid materials~~

设置了格式：字体：Times New Roman

设置了格式：字体：Times New Roman，10 磅

设置了格式：字体：Times New Roman

带格式的：行距：单倍行距，制表位：不在 15.15 字符

induced by severe rain are easily motivated from the source area to the deposit area through the translation area. There burst 6 group debris flow-flash flood disaster chains in rainfall season according to field surveys. Table 1 shows the occurred time, total rainfall of each period, corresponding disaster description, and landslides distribution delineated from remote sensing image data.

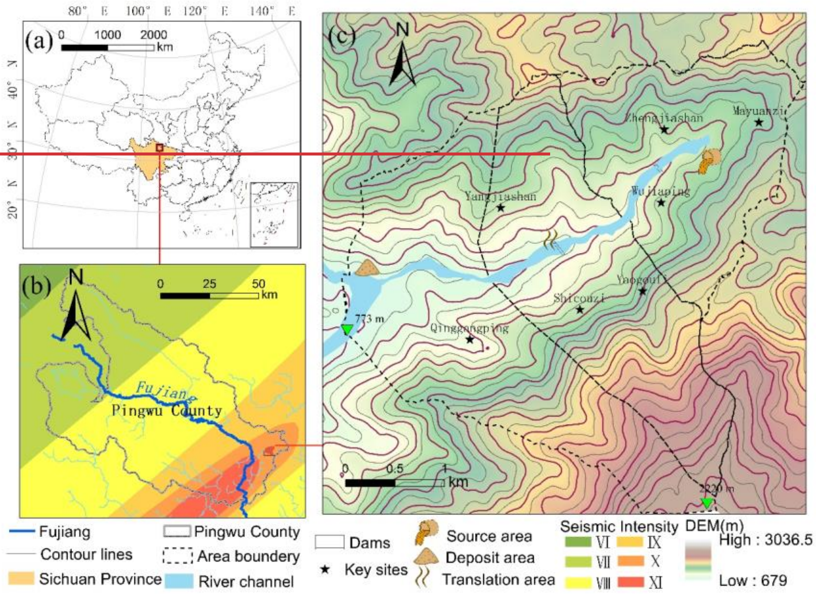

Fig. 1 The location of the study area. (a) Location within China. (b) Location within the seismic intensity ranges of the Wenchuan earthquake. (c) The spatial relationship of the source area, translation area, deposit area, and distribution of elevation.

Table 1 History of hazards in the study area

Time	Total rainfall (mm)	Details	Landslides distribution
2008.9.24	140.0	The debris flows after the earthquake first broke out from Mayuanzi and the deposited sediment was up to 5.0×10^4 m^3 at the junction with the Shikan river, which resulted in collapsed houses and a mess of farmland in the inundation. *	/
2009.7.15-7.16	200.0	The debris flow erupted for 20 min and carried 2.5×10^4 m^3 solid materials into the outlet section in the catchment. *	/
2010.8.13	223.3	Loose materials were carried from branch outlets into the main outlet and deposited in their routes. *	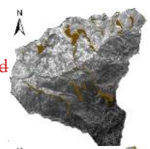
2011.8.20	118.0	The scenario was like in 2010.8.13, while damaged less. *	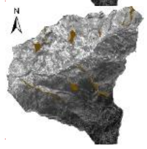

2013.7.7-7.12	800.0	The landslides occurred in the upper steep branch, turning to a rapid and large flow-like motion in the main outlet and sweeping over the houses, pigsty, and arable land near the channel. Eventually, the mixture of soil and fragmented rocks accumulated 29.5×10^4 m^3. *	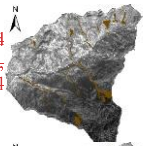
2018.7.9-7.11	360.0	Several branches burst debris flows, and the materials from Qinggang-ping accumulated on the road more than 2 m. *	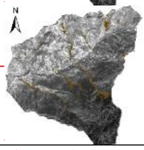

*means the sources are mainly from literature research (Feng et al., 2017; Guo et al., 2018; Zhao et al., 2019)

Vulnerability to landslide hazards is a function of a site's location (topography, geology, drainage), type of activity, and frequency of past landslides (Highland and Bobrowsky, 2008). Consequently, this landscape will not stop experiencing land-slide hazards in the short term. To stabilize the loose solid materials, an engineering control project was completed in October 2010. The project included two blocking dams, one of which was in the upper source area and the other in the translation area (Feng et al., 2017)(Fig. 1(c)). The storage capacity of the two reservoirs are, respectively, 5.78×10^4 m^3 and 7.2×10^4 m^3 and the upper dam (10.0 m) is higher than the other one (9.0 m). With deposited in the reservoirs gradually, the first dredging work was after landslide hazards in 2013 and the upper reservoir remained at half capacity in 2016, meanwhile, the lower reservoir was full of loose material.

3.Six group debris flow-flash flood disaster chains were found in Xingping valley decades after the earthquake. Based on the published work of SKLGP (State Key Laboratory of Geohazard Prevention and Geoenvironment Protection) and the local states' geological survey before 2018 and our biannual field surveys since 2012, we catalogued the time of occurrence, total rainfall of each event, corresponding disaster details in Table S1. The massive sediment was transported quickly after the devastating quake in 2008 and 2009. The extreme rainfall in 2013 and 2018 induced prosperous loose materials deposited in the channel. Considering the landslide processes, we divided the study area into three regions: source area, transitional area, and deposit area (the grey dashed lines in Figure 1c), which meant the loose solid materials would be easily transported from the source area to the deposit one through the transitional zone.

An engineering control project was completed to intercept the upriver materials in October 2010. The project included two check dams, one in the upper source area and the other in the transitional zone (Feng et al., 2017) (Figure 1c). The upper dam has a storage capacity of 5.78×10^4 m^3 and a height of 10.0 m. The transitional area dam has a storage capacity of 7.2×10^4 m^3 and a height of 9.0 m. With the reservoirs gradually filling with deposits, the first dredging work was subsequently done in 2013. Nearly three years later, the storage capacity behind the upper dam remained at 50% in 2016, while the transitional area dam cannot retain sediment.

3 Materials and Methods

带格式的: 行距: 单倍行距

In this study, we examined the intervention effectiveness through the morphological response and sediment yield in the Xing-ping valley, which was simulated using the C-L model. The research entailed four main steps: 1) setting three scenarios varied in intervention compositions, 2) preprocessing the input data including three groups of DEMs, the rainfall data, and m values of the C-L, 3) calibration of the hydrological component, and 4) simulating a three-year of the landscape changes and analysing the intervention effectiveness in 2011-2013.

3.1 Scenarios settings

The abundant source materials ~~of~~triggered by landslides ~~are provided in the quack-stricken area. Control processing~~ should be ~~performed~~controlled to prevent the ~~transportation of loose solid materials. We simulated~~threat of disasters downstream. Therefore, we designed three scenarios incorporating engineering ~~measures~~ and biological measures referenced to current facilities to assess the ~~geomorphic response in 2011-2013 and then assessed the~~ effectiveness of intervention measures. Scenario UP: Unprotected landscapes~~, which means~~ meant the ~~sediment will move with no~~sediments would transport without anthropogenic intervention. Scenario PP: Present protected landscapes~~,~~ implied that only the present two ~~blocking~~check dams ~~stop a large amount of material from moving downslope~~trapped deposits in 2011-2013 without dredging work ~~all~~over the ~~time~~period (see section 2.2). Scenario EP: Enhanced protected landscapes~~, the two blocking dams in Scenario PP~~ emphasised the plus vegetation revetments in the source area and levees in the deposit area~~. The placement~~ based on the two check dams in Scenario PP. Figure 1c shows the locations of the existing two check dams in both Scenario PP and Scenario EP. We determined the placements of additional facilities ~~was decided by~~in Scenario EP according to the ~~annual~~ field survey~~ results, where there are still a large number of materials and the settlements would be damaged every year (see Fig. 2 and Section 3.2.2). The~~ ~~,~~ which demonstrated the continuous supply of sediments was mainly from the source area. Therefore, the vegetation revetments ~~reduce erosion by~~ like trees planting would be carried out upriver for their ability to prevent erosion by stabilising topsoil and enhancing the soil's infiltration capacity ~~of soil and reducing the surface flow velocity. The~~with its roots (Lan et al., 2020). Considering that the flash-flood gushed in and damaged the residential area downriver (see Fig. 2 and Section 3.2.2), the levees are artificial ~~embankments~~barriers to protect ~~the plow~~agricultural land and buildings~~; they are constructed~~, which helped to prevent ~~flow and prevent~~ the ~~mix~~mixture of water and sediment from overflowing and flooding surrounding areas. We simulated and compared the three types of situations described above.

3.2 CAESAR-Lisflood

The C-L model ~~description and setting~~ integrated the Lisflood-FP 2D hydrodynamic flow model (Bates et al., 2010) with the CAESAR landscape evolution model (LEM) (Coulthard et al., 2002; Van De Wiel et al., 2007), which is entirely described in Coulthard et al. (2013). We used the catchment mode that required the surface digital elevation model (DEM), the bedrock DEM, the grain size distribution, and a rainfall time series to simulate the sediment transport and geomorphological changes in this study. The four primary modules operate as follows:

~~The C-L (Tom J Coulthard et al., 2013) was integrated the Lisflood-FP 2D hydrodynamic flow model (Bates et al., 2010) with the CAESAR geomorphic model (T J Coulthard et al., 2002; Van De Wiel et al., 2007), which is based on CA framework to suit the gridded data required in geomorphic processes simulation. Its stronger physical basis in a two-dimensional hydrodynamic flow model and faster simulation in a complete catchment over time scales from hours to thousands of years made it our surface process simulator. The catchment mode requires the surface digital elevation model (DEM), the bedrock DEM, the grain size distribution, the rainfall data and other parameters (Table 2), and related output settings.~~

~~Besides the creative flow model, which is used to simulate the shorter term hydrodynamic effects, there are three main parts hydrological model, erosion and deposition model, and slope progress. The hydrological model uses input rainfall data to generate runoff in the catchment based on adaption of TOPMODEL (Topography based hydrological model) (Beven and Kirkby, 1979), which is routed in flow model including velocity and depth, which are then used to calculate shear stress that can then be used to calculate fluvial erosion and deposition. The slope model enables materials from the slope to be fed into the fluvial system with mass movement occurring when a critical slope threshold is exceeded and soil creep as a function of~~

带格式的：行距：单倍行距

带格式的：缩进：左侧： 0 厘米，首行缩进： 0 厘米，右侧： 0 厘米，段落间距段后：0 磅，行距：单倍行距

带格式的：正文，行距：单倍行距

the slope. These models update variables in square gridded cells at any time interval, such as elevation and derived topographic data, grain sizes and proportion data, hydrological data (e.g., discharge, water depth, velocity), and other types of generalization data.

For three different (1) a hydrological module generates surface runoff from rainfall rates using an adaption of TOPMODEL (Topography based hydrological model) (Beven and Kirkby, 1979),

(2) a hydrodynamic flow routing module based on the Lisflood-FP method (Bates et al., 2010) calculates the flow depths and velocities,

(3) an erosion and deposition module uses hydrodynamic results to drive fluvial erosion by either the Einstein (1950) or the Wilcock et al. (2003) equation applied to each sediment fraction over nine different grain sizes,

(4) and a slope model eliminates materials from the slope to the fluvial system when a critical slope threshold is exceeded.

The C-L model updates variables in square gridded cells at intervals, such as DEM, grain size and proportion data, water depth, and velocity. For three scenarios, we reconstructed four parameters formatted differently in catchment modethe initial conditions, such as DEM,DEMs and bedrock DEM, M, andDEMs, the rainfall series. The arrangements of the input parameters are describeddata, and the m values were reprocessed as follows.

带格式的：缩进：左侧： 0 厘米，首行缩进： 0 厘米，右侧： 0 厘米，行距：单倍行距

3.2.1 Surface and bedrock digital elevation model

设置了格式：字体：10 磅，加粗，字体颜色：黑色

Although the run time of the C-L simulation increases exponentially as the number of grid cells increases, to describe clearly the control process, especially the two dams and levees in the catchment, we unified grid cell scales to 10 m for all needed data. The GlobalDEM product with a 10 m × 10 m resolution and 5 m (absolute) vertical accuracy was used as the prepared data to form three types of initial DEMs (UP DEM, PP DEM, and EP DEM). Before rebuilding initial DEMs, we filled the sinks of the original GlobalDEM, which were prone based on Environmental Systems Research Institute's (ESRI's) ArcMap (ArcGIS, 10.8) to form by interpolation operation, and then causedeliminate the hydrological module to calculate inconsequently. The'walls' and the 'depressions' in the cells and avoided the intense erosion or deposition in the early run time. Then the non-sinks DEM could bewas used as the surface DEM of the unprotected landscapes in Scenario UP (UP DEM) in 2011.without any facilities. According to the engineering control project described in Section 3.2.2, present protected landscapes'Scenario PP's surface DEM (PP DEM) was added 10included the dams by raising the grid cell elevations by 10 m for the upper dam and 9 m for the dam in the location of dams, respectivelytransitional area. Similarly, the enhanced protected landscapes' surface DEM in Scenario EP (EP DEM) was extracted by increasing the value of specified grid cells which would be expressed levees building based on included the dams in PP DEM. And the height of the levees wasIn addition, two levees were produced by raising grid cells' elevation by 2 m, an average height used in the lower river channel of the study area to prevent high and fast flow. that were represented at selected locations. Incidentally, the placement and setting of vegetation revetments in Scenario EP were introduced in Section 3.2.2.

From the field survey and the contents of sectionIn Section 2.2, the spatial distributionheterogeneity of source materials indicates the discrepancy of erodible thickness (, which equals the difference between surface DEM (DEM) and bedrock DEM) was different. The bedrock DEM included in this model for each scenario to stop eroding was derived by subtracting (bed-DEM). We divided the erodible thickness from surface DEM. The distribution of erodible thickness was divided into five regions (Fig. 2) by comparingS2) by checking out the foundationrelative elevation of the foundations of buildings, the exposed bedrock, and the residents' memory of the history of deposited depth of landslides deposited.to the ground level. The average thicknesses of upstream low and high-altitude areas were set to 10 m and 3 m, respectively, and the erodible layer in the downstream area was supposed to be 3 m. For the river channel and outlet, there would be a large amount of deposition, and there were supposedthe thickness of erodible sediment was set to be 5 m and 4 m approximately. The engineering control processes with two , respectively. The dams in Scenario PP and two dams cooperated with the levees in Scenario EP were supposed to be non-erosive concrete. SoAs such, we set the erodible thickness of the engineering control processes area was these features to 0 m. Fig. 2 shows the flow chart of the generation ofEventually, DEMs and bedDEMs. In addition, all of the DEM were formatted to ASCII raster as required in C-L.

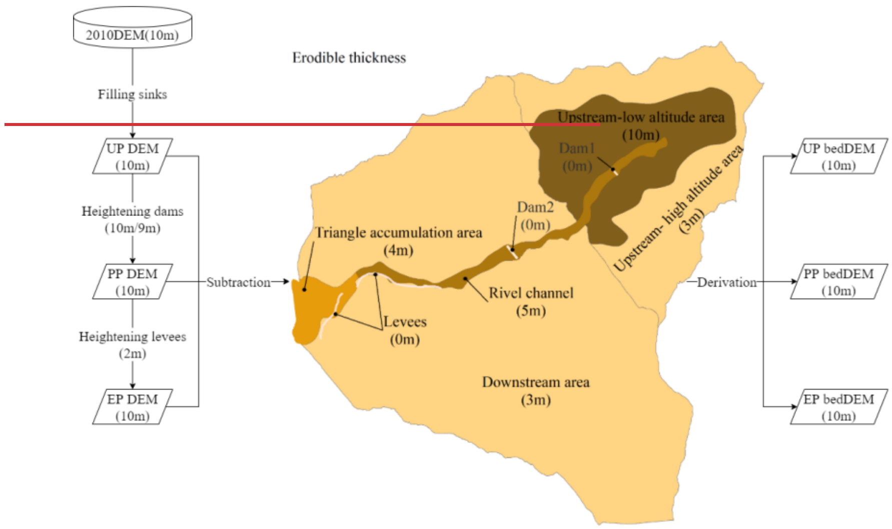

Fig. 2 Flow chart describing by C-L. The divided regions varied in erodible thickness, the placement of additional levees and vegetable revetments in Scenario EP, and the generation process of DEMs and bedDEMs (bedDEM: bedrock DEM). All the numbers attached to DEM on both sides indicated the DEM grid's width and the numbers under facilities such as dams on the left one are height measured from surface DEM. The numbers in central erodible thickness are the depth of the material which is capable to remove by runoff.were shown in Fig. S3.

3.2.2 Vegetation settings

Another parameter in scenarios used in simulations was “m” which controlled the exponential decline of transmissivity with depth (Batty et al., 1997) and influenced the peak and duration of the hydrograph in response to rainfall. The lower the value of “m”, the lower the vegetation coverage, the flashier flood peaks, and the shorter duration hydrographs. In this research, the “m” in UP and PP scenarios were set to 0.008 without spatial variation, which represented that the vegetation coverage is similar to farmland referenced to research in the same study area by Li et al., (2020). As mentioned earlier, the upstream-low attitude area covered by the biological measures designed in the EP scenario indicated a high value of “m”. To distinguish the “m” in the biological protected area clearly, the “m” was set to 0.02, equal to the vegetation coverage in the forest (Li et al., 2020).

Another parameter required in each scenario was the m value in C-L's hydrological model (TOPMODEL), which controls the exponential decline of transmissivity with depth (Beven, 1995, 1997) and influences the peak and duration of the hydrograph

带格式的：左，缩进：左侧： 0 厘米，右侧： 0 厘米，段落间距段后：0 磅，行距：单倍行距

设置了格式：字体：10 磅

设置了格式：字体：10 磅

设置了格式：字体：10 磅，加粗，字体颜色：黑色

in response to rainfall. The lower the m value, the lower the vegetation coverage, and the flashier flood peak and shorter duration are reflected in the flood hydrograph (Coulthard et al., 2002). The m value is usually determined by the landcover (e.g., 0.02 for the forest, 0.005 for the grassland) (Coulthard and Van De Wiel, 2017). In our study, we set the value as 0.008 in our smaller catchment (14 km^2) in Scenario UP and PP, which resembles the m value of farmland covered with lower vegetation in the same catchment studied by Xie et al. (2018) and Li et al. (2018). As mentioned earlier, the upstream-low elevation area covered by the biological measures designed in the EP scenario was assigned a higher m value of 0.02. It has been calibrated in the more extensive catchment containing our study area by replicating the flood event in 2013 (Xie et al., 2018).

3.2.3 Rainfall data

设置了格式：字体：10 磅，加粗，字体颜色：黑色

带格式的：缩进：左侧： 0 厘米，行距：单倍行距，孤行控制，制表位：不在 2.13 字符

In this research, we compared three scenarios usingwith identical precipitation data duringbetween 2011 and 2013, as mentioned in section 3.1. The source data of precipitation in 2011-2013 (Fig. 3((Figure 4a))) was downloaded from the China Meteorological Administration (http://data.cma.cn()http://data.cma.cn, with daily temporal resolution. The rainfall intensity and the frequency of extreme events affect patterns of erosion and deposition (Tom J. Coulthard et al., 2012), therefore, we used the stochastic downscaling method to generate hourly data to best capture the hydrological events in this study, which was introduced by Li et al., (2020) and Lee and Jeong, (2014). The referenced hourly precipitation was from the pluviometer located 20 km from the study area in 2016(Fig. 3(b)), with annual total precipitation of 684 mm. The rainfall in 2016 was characterized by (1) hourly precipitation from 1.1 mm to 35.4 mm and (2) the maximum and average duration of a rainfall event up to 24 h and 2.8 h. In the downscaling method, the daily rainfall was divided into four levels (>100 mm, 50-100 mm, 20-50 mm, and 0-20 mm) and the referenced hourly rainfall series of those days whose daily rainfalls were close to the value on the day at a certain level were combined by reproduced, crossed and mutated included in the genetic algorithm (Goldberg, 1989). At last, the downscaled rainfall series were generated by gathering the normalized hourly data based on the daily rainfall. Fig. 3(c) shows the downscaled rainfall series in 2011-2013, which illustrated that the downscaled hourly precipitation series was better than the hourly-mean precipitation (5.27 mm) in the day with maximum precipitation (126.5 mm).

设置了格式：无下划线，下划线颜色：自动设置

设置了格式：下划线

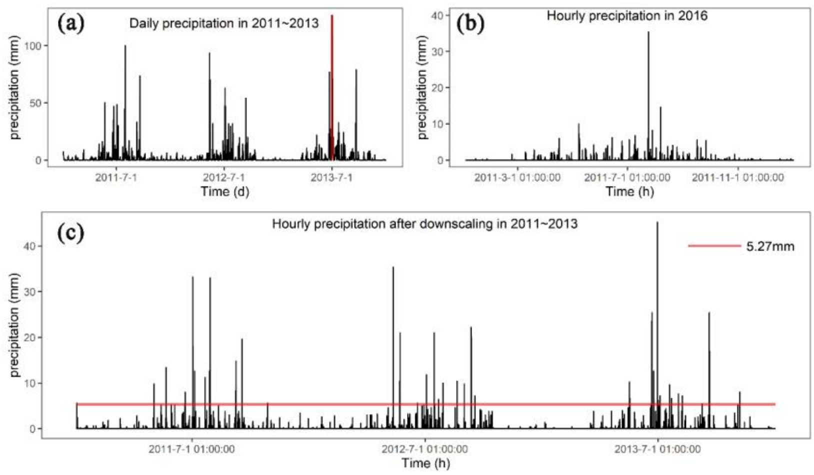

Fig. 3(a) showed the required downscaling daily) with daily temporal resolution. The rainfall intensity and the frequency of extreme events affect patterns of erosion and deposition (Coulthard et al., 2012b; Coulthard and Skinner, 2016). Therefore, we used the stochastic downscaling method to generate hourly data to best capture the hydrological events in this study, which was introduced by Li et al. (2020) and Lee and Jeong (2014). The referenced hourly precipitation was from the pluviometer located 20 km from the study area in 2016 (Figure 4b), with an annual total precipitation of 684 mm. The rainfall in 2016 was characterised by that (1) hourly precipitation was from 1.1 mm to 35.4 mm, and (2) the maximum and average duration of a rainfall event was 24 h and 2.8 h, respectively. The main processes of the downscaling method are:

- extracting the hourly rainfall of specific days in 2016 closest to the daily rainfall in 2011-2013 through the threshold setting and producing the genetic operators using the extracted hourly rainfall dataset;
- mixing on the genetic operators by genetic algorithm (Goldberg, 1989) composed of reproduction, crossover and mutation and repeating until the distance between the sum of hourly rainfall and the actual daily rainfall is less than the set threshold;
- normalising the hourly precipitation to remain the daily rainfall value unchanged. The input of generated hourly precipitation is catchment lumped in Scenario UP and PP and divided into two separate but identical rainfall in Scenario EP.

Figure 4c shows the downscaled rainfall series between 2011 and 2013. The downscaled hourly precipitation better captured the hydrological events on account of the hourly-mean rain (5.27 mm) in the day with extreme rainfall (126.5 mm), which was far from the actual situation.

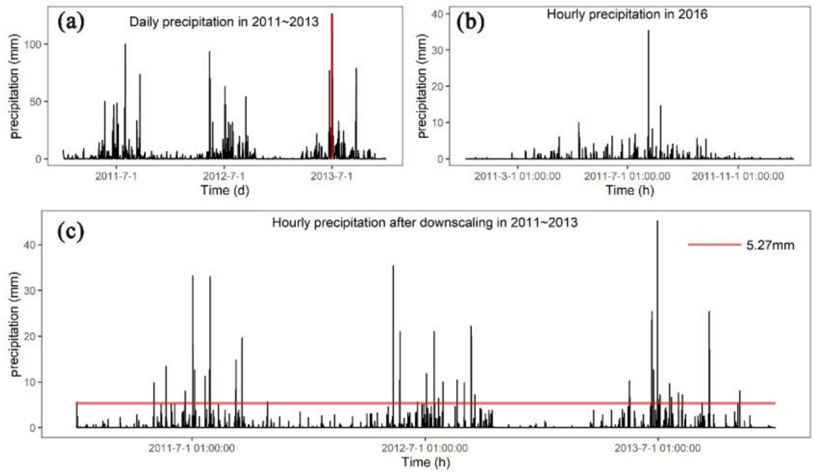

Figure 4: (a) Daily precipitation in 2011-2013 (the red vertical line indicates daily maximum daily precipitation of 126.5 mm); (b) showed the referenced hourlyHourly precipitation in 2016; (c) showed the downscaledDownscaled hourly precipitation in 2011-2013 (the red horizontal line indicates the hourly-mean precipitation 5.27 mm in the day with maximum precipitation showed in (a))).

带格式的: Captions, 行距: 单倍行距

3.2.4 Other parameters

设置了格式: 字体: 10 磅, 加粗, 字体颜色: 黑色

带格式的: 缩进: 左侧: 0 厘米, 行距: 单倍行距, 孤行控制, 制表位: 不在 2.13 字符

The C-L model is sensitive to a set of model physically based parameters included in Skinner et al., (2018) for an identical catchment with a grid cell size of 10 m, such as slope for edge cells, grain size set, vegetation critical shear stress, and Manning's n values. These parameters were determined by the application of Xie et al., (2018) and Li et al., (2020) in the same study area. In particular, the Manning' n roughness was set according to suggested values (Arcement and Schneider, 1989) in different land-use, and other more sensitive parameters were determined by repeated experiments such as the minimum Q value (see Table 2).

Table 2 The C-L parameter values for the simulations of three different scenarios.

The C-L model is sensitive to a set of input data introduced by Skinner et al. (2018) for a catchment with a grid cell size of 10 m, such as sediment transport formula, slope failure threshold, and grain size set. The grainsize distribution of sediment is derived from samplings at 14 representative locations in the same study basin by Xie et al. (2018). Given the grainsize distribution in this study, we selected the Wilcock and Crowe formula as the sediment transport rule, which was developed from flume experiments using five different sand-gravel mixtures with grain sizes ranging between 0.5 and 64 mm (Wilcock et al., 2003). Considering the steep slope on both sides of deep gullies there distribute, we tended to set a higher slope failure threshold to replicate the geomorphic changes between 2011 and 2013 realistically. Additionally, we found that the probability of shallow landslides indeed accumulated from 20°to 50° in slope gradient between 2011 and 2013 (Li et al., 2018). The slope angle was derivate from the DEM with a 30 m spatial resolution, which caused a lower slope angle than that with a 10 m resolution. As such, we set 60°, which is lower than the 65° used in a scenario without landslides (Xie et al., 2022) and higher than 50°. Some parameters were determined by repeated experiments such as the minimum Q value and the other input values were referred to default values recommended by the developers (such as the max erode limit in the erosion/deposition module and the vegetation critical shear stress) in https://sourceforge.net/p/caesar-lisflood/wiki/Home/.Table S2 in the supplemental material presented C-L model parameters used in the current study.

3.2.5 Model calibration

Considering the ungauged basins before 2015, we replicated the flash flood event in July 2018 by C-L to calibrate the hydrological components. Based on Scenario PP (with two check dams), we changed the rainfall series into the two-week hourly precipitation in July 2018 (Fig. S2a), which is recorded by the rain gauge 2.5 km away from the catchment (Fig. S2b). The simulation results (Fig. S2c and Fig. S2d) represented the erosion map and maximum water depth map in Scenario PP on July 15, 2018. As shown in Fig. S2c and Fig. S2d, we selected three locations to compare the simulation results with remotely sensed images and photos. The comparative results (Fig. S3) revealed the similar ranges of the deposition and inundation between simulation results and remotely sensed images. Additionally, the values of simulated sediment depth and water depth were close to those measured from images, which indicated that the flash flood event was replicated successfully by the C-L using the input data.

Table 1 shows three-year landscape changes under three different scenarios that were simulated and compared to analyse the intervention effectiveness in 2011-2013.

Table 1: Scenarios setting

~~Parameters~~**Scenario**	~~Value~~**Descriptions**	~~Description~~**Period**	**DEM (10m)**	**Rainfall data**
~~9 kinds of grainsizes (m) (grainsize proportion) ★★~~	~~0.000074(0.098), 0.0005(0.138), 0.001(0.052), 0.002(0.162), 0.005(0.158), 0.01(0.169), 0.02(0.13), 0.04(0.06), 0.1(0.033)~~	~~Used for calculating the sediment transport in each active layer~~		
~~Suspended fall velocity(m/s)~~UP	~~0.0003~~no anthropogenic intervention	2011-2013 (3 years)	UP DEM UP bedDEM	~~Designated as the falling velocity for the finest fraction(74μm)~~ downscaled hourly precipitation in the period (lumped)

插入的单元格
设置了格式：字体：9 磅，加粗
插入的单元格
带格式的：正文，行距：固定值 12 磅
设置了格式：字体：9 磅，加粗
设置了格式：字体：9 磅，加粗
合并的单元格
插入的单元格
插入的单元格
设置了格式：字体：9 磅
带格式的：正文，行距：固定值 12 磅
设置了格式：字体：9 磅
带格式的：正文，行距：固定值 12 磅
设置了格式：字体：9 磅

Sediment transport formula ★★★★	Wilcock and Crowe	A criterion calculated the fluvial erosion and deposition for all cells	
Max erode limit (m) ★★★	0.002	The maximum amount of material that can be eroded within a cell at each time step	
In channel lateral erosion rate ★★★	20	Controlling the channel narrowing	
Active layer thickness (m)	0.1	The thickness of a single active layer	
Lateral erosion rate ★	0.000003	The variable controls lateral erosion	
Lateral edge smoothing passesPP 40	The number of passes for the edge smoothing filter (distance between two meanders)the present two check dams upstream without dredging work	PP DEM PP bedDEM	
Vegetation critical shear stress (Pa) ★★★	100	The value above which vegetation would be removed by fluvial erosion	
Grass maturity rate (yr) ★	1	The speed at which vegetation reaches full maturity in years	
The proportion of erosion that can occur when vegetation is fully grown EP 0.1	Determined the effects ofadditional vegetation maturity on "revetments in channel lateral erosion rate"the source area and levees in the "lateral erosion rate".deposit area based on Scenario PP	EP DEM EP bedDEM	downscaled hourly precipitation in the period (spilt)
Soil creep rate(m/yr) ★★	0.0025	The variable tends to cause erosion gradually on sharper features in the terrain	
Slope failure threshold (°) ★★★	60	Angle threshold in degrees above which landslide occur	
Input/output difference allowed(m^3/s) ★★	0.5	Described the flow model running in a steady state and used to speed up the model operation	
Min Q for depth calculate(m) ★★★	0.1	The value above which the flow depth would be calculated to save running time	
Water depth threshold above which erosion will happen(m)	0.01	The value above which the model starts to calculate erosion	
The slope for edge cells ★★	0.005	The exit cells' slope to control the erosion and deposition	
Evaporation rate (m/d) ★★★	0.00418	Used to calculate the evapotranspiration	

删除的单元格
带格式的：正文，行距：固定值 12 磅
带格式的：正文，行距：固定值 12 磅
插入的单元格
插入的单元格
插入的单元格
设置了格式：字体：9 磅
设置了格式：字体：9 磅
删除的单元格
带格式的：正文，行距：固定值 12 磅
设置了格式：字体：9 磅
带格式的：正文，行距：固定值 12 磅
设置了格式：字体：9 磅
插入的单元格
插入的单元格
插入的单元格
设置了格式：字体：9 磅
设置了格式：字体：9 磅
设置了格式：字体：9 磅
设置了格式：字体：9 磅

~~Courant number~~	~~0.3~~	~~The value controls the numerical stability and speed of operation of the flow model~~
~~Manning's n values (forest, river channel, landslides, farmland, grassland, buildings) ★★~~	~~0.07, 0.045, 0.04, 0.035,0.03,0.015~~	~~The roughness coefficient used by the flow model~~

~~Note: The greater the number of ★, the more sensitive to the model, and the unlabeled parameters were not studied (Skinner et al., 2018).~~

3.3 Output ~~analyses~~analysis

~~The overall temporal and spatial changes in internal geomorphology under three different scenarios were available to assess intervention measure effectiveness. The simulated elevation changes on the last day of each year were selected to show the details, which were derived from the~~ The C-L model outputs in each scenario include hourly discharge at the basin outlet, the difference between ~~output~~ DEMs at a specified time and initial DEMs (EleDiffs~~). The~~), and hourly sediment yield. We validated the model outputs by comparing the hourly discharge and EleDiffs ~~indicated~~reflecting the depth of sediment deposition or erosion (> 0.1 m: deposition, < 0.1 m: erosion~~). We classified the depth to show the distribution of the deposition and erosion, defined the total damaged area in each scenario by summing all affected cells' areas, and compared the damaged area of every classification in three scenarios. In addition, we zoomed in on the key spots including blocking dams, levees, and vegetation revetments to explore the~~) with field survey materials. The overall temporal and spatial geomorphic changes reflected by EleDiffs under three different scenarios were used to assess the geomorphic response to interventions. To explore the response to various control measures ~~in different scenarios and record the depth of deposition in dams blocking areas. To quantify the changes in the internal source area, translation area, and deposition area, the sediment~~, we zoomed in on the key spots placed checking dams, levees, and vegetation revetments and recorded the depth of deposited sediment behind two dams. For further exploring the spatial heterogeneity, we compared respectively with the volumes of deposition and erosion ~~were calculated respectively from the EleDiffs cuboid.~~

~~In different scenarios with different intervention measures, the~~ in three divided regions ~~would behave differently in sediment conservation. To quantify~~, including the source area, transitional area, and deposition area.

Based on the visual and quantitative results, we defined two formulae to assess the intervention's effectiveness. The conservation ability ~~conveniently, we defined some related~~ (*Ca*, Eq. (3)) was based on variables ~~based on~~in the sediment balance system ~~(Fig. 4). In the balance system, for the region *n*, the~~(Figure 5). The sediment volume of deposited sediment (~~D_n~~D_n) and ~~the~~ input sediment from the upper connected region (~~I_n) are~~I_n) is equal to ~~the~~that of eroded material ~~volume (E_n) plus the~~(E_n) and output ~~volume~~sediment to the next ~~region (O_n) in~~part (O_n) over the same period. ~~Based on the relationship between variables shown in Eq.1 and~~ (Eq.~~2, we defined C_a~~ (1), Eq. ~~3) to quantify the sediment conservation ability~~(2)) in the system. A higher value of *Ca* in a specific region and scenario indicates that a more effective control system is applied.

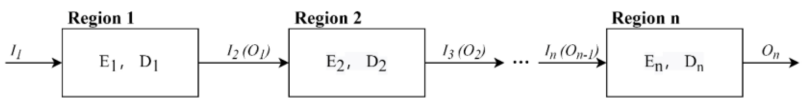

带格式的: 行距: 单倍行距

带格式的: 缩进: 左侧: 0 厘米, 首行缩进: 0 厘米, 右侧: 0 厘米, 行距: 单倍行距

带格式的: 与下段同页

~~Fig. 4.~~Figure 5: The sediment balance system in the study area (the Region *n* indicated source area, ~~translation~~transitional area, and deposit area in this study)

$$I_n = \sum_{2}^{n} E_{n-1} - \sum_{2}^{n} D_{n-1}, \quad (1)$$

$$I_n + E_n = O_n + D_n, \quad (2)$$

$$Ca = \frac{D_n}{I_n + E_n} \quad (3)$$

Where, *n* is the region number of source area (=1), ~~translation~~transitional area (=2), and deposit area (=3).

~~The daily sediment yield measured in the valley was the other important output variable of sediment transport. We referenced a terminology from the stock market in economics to assess the relative efficiency (Eq. 4, compared with Scenario UP) of engineering protections in scenario PP and engineering cooperation with biological measures in scenario EP.~~

Additionally, we designed the relative efficiency (*Re*, Eq. (4)) to depict how much a set of intervention measures in Scenario PP and EP were efficient in sediment loss, with the comparison to Scenario UP.

$$Re_{PP/EP,i} = \frac{Q_{UP,i} - Q_{PP/EP,i}}{Q_{UP,i}} \quad (4)$$

Where *i* is the sequence of the day; $Q_{UP,i}$ is the daily sediment yield ~~volume from~~measured at the catchment outlet in Scenario UP~~ of day *i*~~; $Q_{PP/EP,i}$ is the daily sediment yield ~~volume from~~measured at the catchment outlet in Scenario PP or Scenario EP of day *i*; $Re_{PP/EP,i}$ is daily relative effectiveness of ~~controlling~~control measures in Scenario PP or -Scenario EP~~ of day *i*~~.

4. Results

4.1 Model verification

Figure 6 shows the input precipitations and modelled discharge hydrograph between 2011 and 2013 (Figure 6a), in addition, presents the comparison of simulated mean discharge in April through July and the whole year with field survey materials in two locations (Figure 6 b, c). Concerning the discharge hydrograph, the peak discharges (63.7, 54.9, and 50.3 m^3/s) appear identically with the peak rainfall intensities (31, 19.7 and 15 mm). The value of modelled discharge from March to May in the catchment outlet (location A) is slightly larger than the measured value recorded by Feng et al. (2017). Additionally, an average annual discharge of 10.04 m^3/s in location A is less than that of 12.80 m^3/s in the catchment outlet (location B), which has an area approximately three times the study area.

带格式的: Captions

带格式的: 左, 段落间距段前: 6 磅, 段后: 6 磅, 行距: 单倍行距

格式化表格

带格式的: 左, 段落间距段前: 6 磅, 段后: 6 磅, 行距: 单倍行距

带格式的: 左, 段落间距段前: 6 磅, 段后: 6 磅, 行距: 单倍行距

设置了格式: 字体: (中文) 宋体, 倾斜

带格式的: 缩进: 左侧: 0 厘米, 右侧: 0 厘米, 段落间距段后: 0 磅, 行距: 单倍行距

带格式的: 段落间距段前: 6 磅, 段后: 6 磅, 行距: 单倍行距

格式化表格

带格式的: 左, 段落间距段前: 6 磅, 段后: 6 磅, 行距: 单倍行距

带格式的: 缩进: 左侧: 0 厘米, 右侧: 0 厘米, 段落间距段后: 0 磅, 行距: 单倍行距

设置了格式: 字体: Times New Roman, 加粗

带格式的: 缩进: 左侧: 0 厘米, 行距: 单倍行距

设置了格式: 字体: Times New Roman

设置了格式: 字体: Times New Roman, 10 磅

设置了格式: 字体: Times New Roman

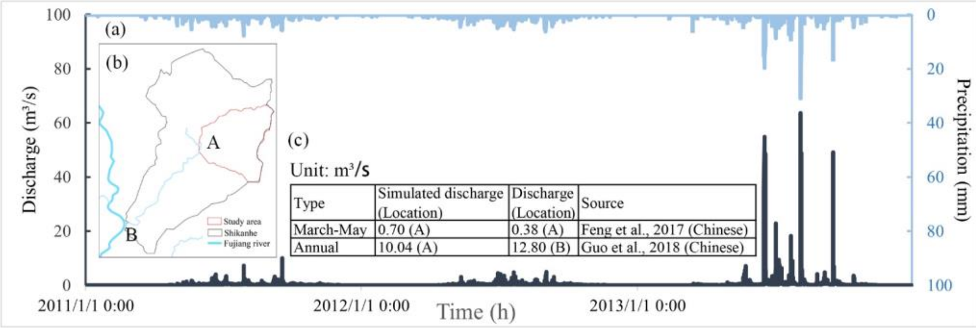

Figure 6: (a) The input hourly precipitation and simulated discharge in 2011-2013 in Scenario PP; (b) the specified locations to verify; (c) the comparison of the simulated average discharge to the recorded discharge.

Figure 7 compares typical cross-sections to the site photos based on the replicated landscape changes in Scenario PP. The first site is on the upriver road, which was eroded to a depth of 5 m according to the simulation results, while the photo shows a depth of no less than 4.0 m without an apparent eroded base. The cross-section and site photo of the gully labelled 2 depict that the eroded depth is approximately 1.0 m. Meanwhile, a clear sediment boundary is found in the building located at the deposited area, indicating a slightly lower deposition depth than the modelled one.

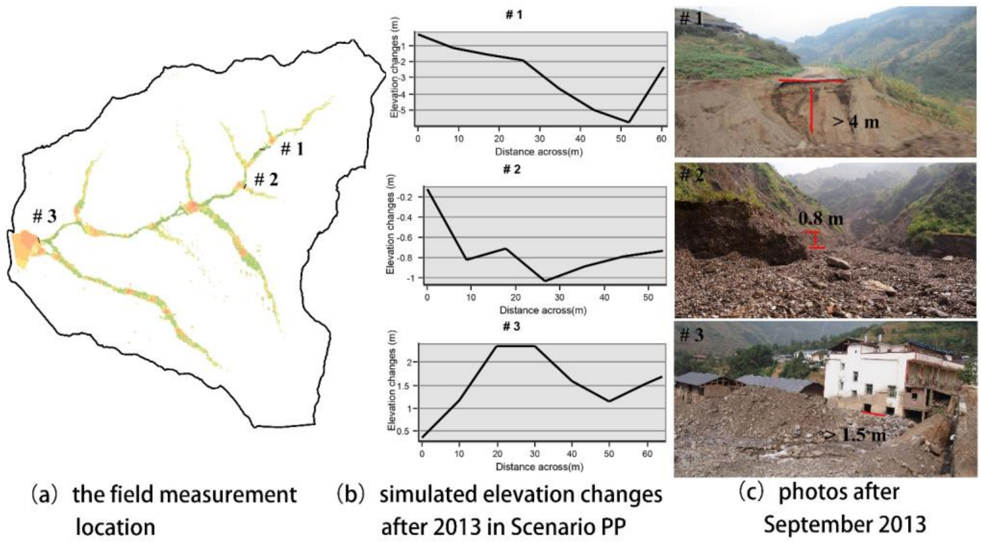

Figure 7: The comparison of cross-sections from the simulation results to the photos in the field measurement locations after 2013 in Scenario PP.

4.2 Overall geomorphic changes

带格式的: 行距: 单倍行距, 制表位: 不在 11.22 字符

~~There were three panoramas at the end of each year~~ Figure 8a shows the three annual landscapes changes in each scenario, which were classified into seven ranks by natural breaks for EleDiffs ~~(Fig. 5):~~: extreme erosion ~~(-15-10~~(<-7 m), heavy erosion (-~~10~~-7--3 m), moderate erosion (-~~7~~-3--1 m), light erosion ~~(-3--~~(1-0.1 m), micro change (-0.1-0.1 m), light deposition (0.1-~~3~~1 m), moderate deposition (1-3-~~7~~ m), heavy deposition (3-7-~~10~~ m), and extreme deposition ~~(10-14 m). The erosion and deposition aggravated in a~~(>7 m). A similar spatial pattern of erosion is observed in all three scenarios. ~~Erosion~~ In detail, erosion occurred mainly in the ~~upper reaches of the~~ main channel and the branches on both sides, among which the left branches were extremely serious, such as Qinggangping gully and Shieaozi gully. As shown in Fig. 5, the three scenarios appeared to have different severe. In contrast, the deposition distribution patternsappeared to be varied in three scenarios, especially aroundbe-hind the two dams. Statistically, the Scenario UP damaged showed in Scenario PP and EP.

The total area of affected grid cells representing erosion and deposition in each scenario was calculated to reveal the difference (Figure 8b). As shown in Figure 8b, the affected area in Scenario UP was the largest at about 0.76 km^2 (5.4% of the total catchment), the PP affected which was larger than that in Scenario PP (0.70 km^2 (, 5.0% of the totalwhole catchment), and the EParea decreased the area to 0.61 km^2 (4.4% of the total catchment).) in Scenario EP. The damagedtotal area of erosion and deposition reduced gradually as the more controlling measures for loose solid materialswere established in this study.

带格式的：缩进：左侧： 0 厘米，首行缩进： 0 厘米，右侧： 0 厘米，行距：单倍行距

In addition,Figure 8c compares the affected areaextent of seven ranksgeomorphic changes showed different effects in three situations using the different scenariosareas varied in depth. Erosion in the three scenarios was similar in that the light and the moderate erosion areas were more than the area of extreme and heavy erosion areas. The area of each erosion degree in UP was almost largermore extensive than that in PP and both larger than that in EP, except that the light erosion area in PP was slightly larger than that in the UP. For the deposition in the internal geography. In addition, the greater the deposition depth, the less deposition coverage of deposition.. Especially, the extreme deposition area was slightlysomewhat more than the area of the heavy deposition in UP. Further analysis showedshows that the extreme, moderate, and light deposition areas decreased to varying degrees in the order of UP, PP, and EP, and the. The heavy deposition areas showedshow the opposite trend, which mainly contributedcontributing to the blocking ofchecking dams and vegetation revetmentrevetments.

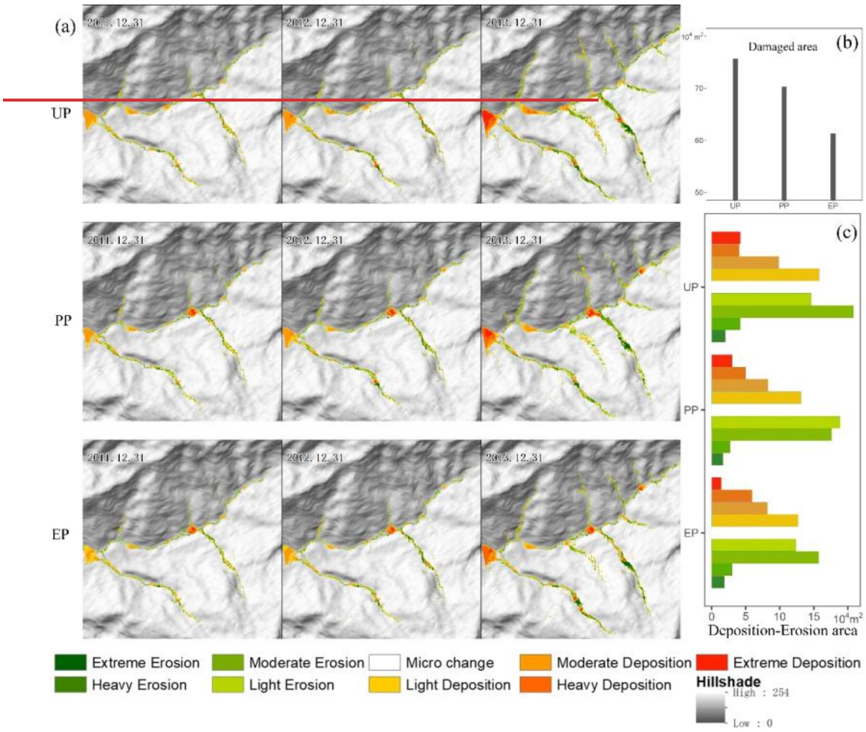

Fig. 5.

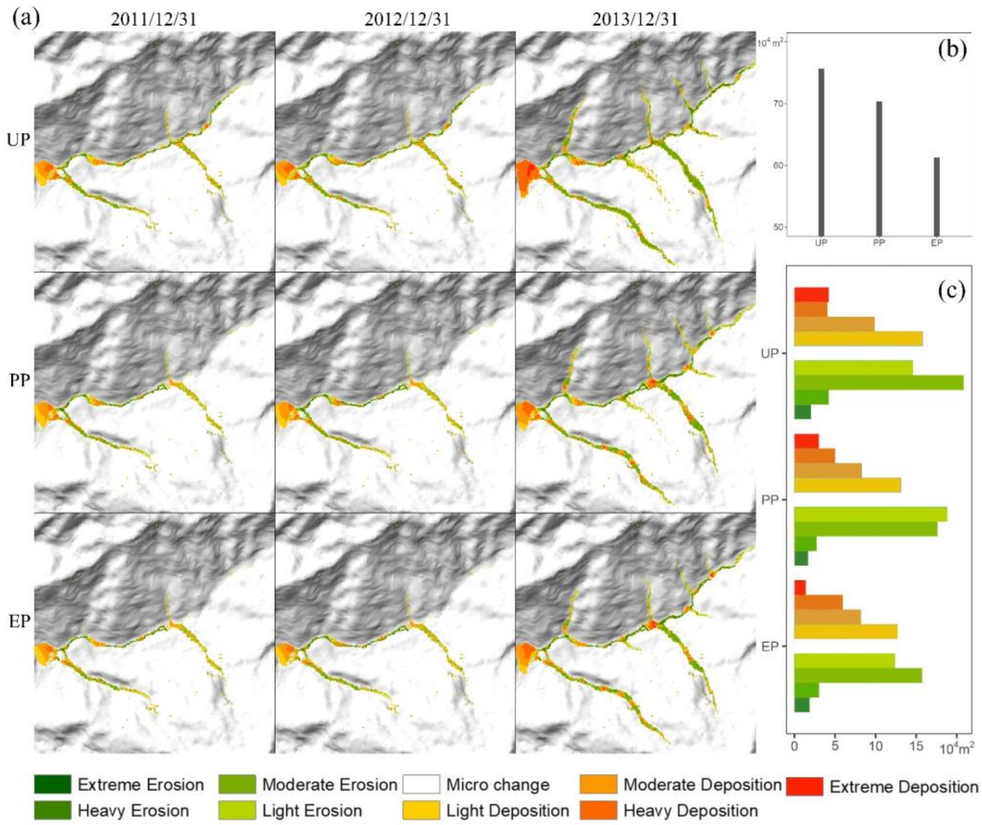

Figure 8: (a) Simulated internal geomorphic changes over time for three scenarios; (b) the ~~damaged~~affected area included deposition and erosion for three scenarios; (c) the ~~final different~~ ranks of deposition and erosion for three scenarios.

4.~~2~~3 Details of key spots

~~An amplified~~ As shown in Figure 9, we provide a detailed investigation of the controlling measures ~~around their position detailed the differences in~~ and surroundings for the three scenarios. ~~Therefore, the upriver land panorama, containing~~ Behind the two dams ~~in Scenario PP and cooperating with extra biological measures in Scenario EP, was used to outline the affected area, measure the impacts on blocking sediment, and examine how the biological area helped to stabilize the slope. Similarly, the panorama of downriver land described the two levees in scenario EP escape from the debris, protecting the plow lands and buildings.~~

~~In the~~ upriver ~~reservoirs of the two dams (Fig. 6),~~, the evident orange clusters ~~indicated the accumulation in Scenario PP and EP, whereas erosion showed in green in the scenario UP. The area of accumulation blocked by dam 1 in EP was similar to PP's area while the accumulation in EP covered a larger range than~~indicate that ~~in PP blocked by dam 2.~~ the deposition appeared in Scenario PP and EP. In contrast, these locations were dominated by erosion, shown in green in scenario UP. Further analysis ~~(Fig. 7) about~~of the sediment depth ~~of deposition blocked by two dams~~ shown in Figure 10 showed that the values of deposited depth ~~blocked by dam 2 was larger than that blocked by dam 1~~behind the dams in Scenario EP were lower than those in Scenario PP. Additionally, in Scenario ~~UP and PP. Whereas, the deposition depth blocked by dam 2 decreased to be slightly~~

带格式的：Captions，左，缩进：左侧： 0 厘米，右侧： 0 厘米，段落间距段后：0 磅，行距：单倍行距

设置了格式：字体：Times New Roman，10 磅

设置了格式：字体：Times New Roman

带格式的：行距：单倍行距，制表位：不在 12.12 字符

带格式的：缩进：左侧： 0 厘米，首行缩进： 0 厘米，右侧： 0 厘米，行距：单倍行距

lower than that by dam 1 in Scenario EP. In Scenario PP, thePP, sediment depth blockedtrapped by dam 1 was largerlower than the height of the dam body at the end of simulation time. Similarly, the accumulation blockedthat by dam 2, but both with more than 10 m-deposition exceeded the damdams' heights (the dam 1's height is 10 m, the dam 2's height at last. Inis 9 m) finally. At the conclusion of the simulation in Scenario EP, both the reservoir areas of dam 1 and dam 2the values of depth behind the two dams were nearly 8 m, which were lower than the dams' heightdams' heights.

The materials produced from upriver tributary gullies varied in three scenarios by the extraadditional biological protection measures. There yielded in three scenarios. A volume of 14.4×10⁴ m³ loose materials in EP'ssediments was transported from EP's biological protection area (solid lines in Fig. 6). In the same gullies, theFigure 9). The loose materials were 27.1×10⁴ m³ and 16.9×10⁴ m³, respectively, were produced in the same region without biological protection in Scenario UP and PP without biological protection.. The vegetation revetment enhanced the sediment conservation based on the role of dam 1. In addition, the materials were carried mainly from the two gullies in the upriver of dam 2 and the downriver of biological protection area, which was inferred from the larger amount of erosion volumes in two gullies in each scenario (48.2×10⁴ m³, 42.5×10⁴ m³ and 35.2×10⁴ m³ in Scenario UP, PP, and EP).

In the downriver area, the levees had an important role in preventing debris and protecting the property. Compared with the accumulationdeposition in UP and PP without levees, in the downriver area shown in the bottom row of Figure 9, the levees in EP blocked debris in the bend of the channel and protectedplayed an essential role in protecting the residents and cultivated land alongbehind the riverlevees.

带格式的：缩进：左侧： 0 厘米，首行缩进： 0 厘米，右侧： 0 厘米，行距：单倍行距

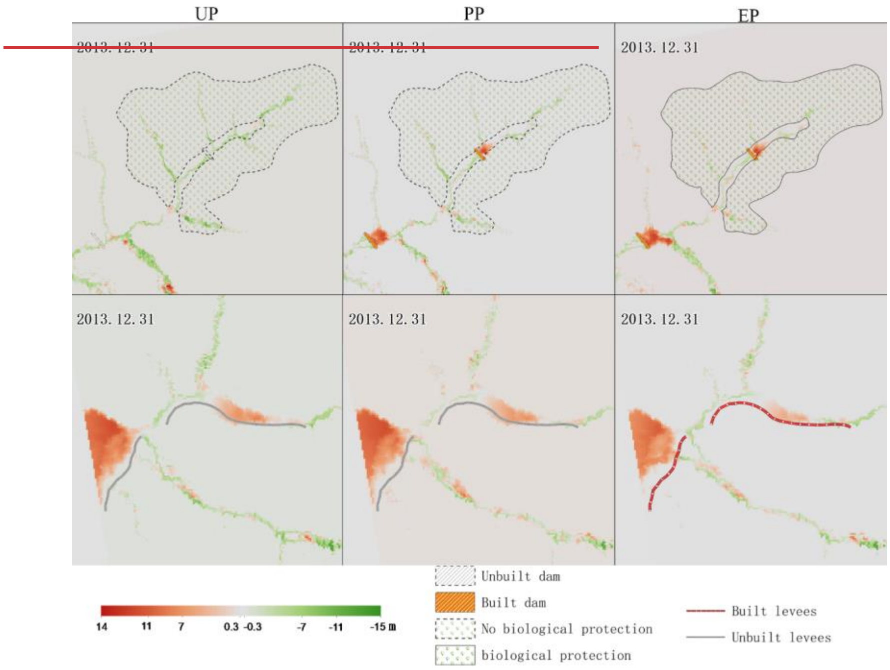

Fig. 6. The final detailed geomorphic

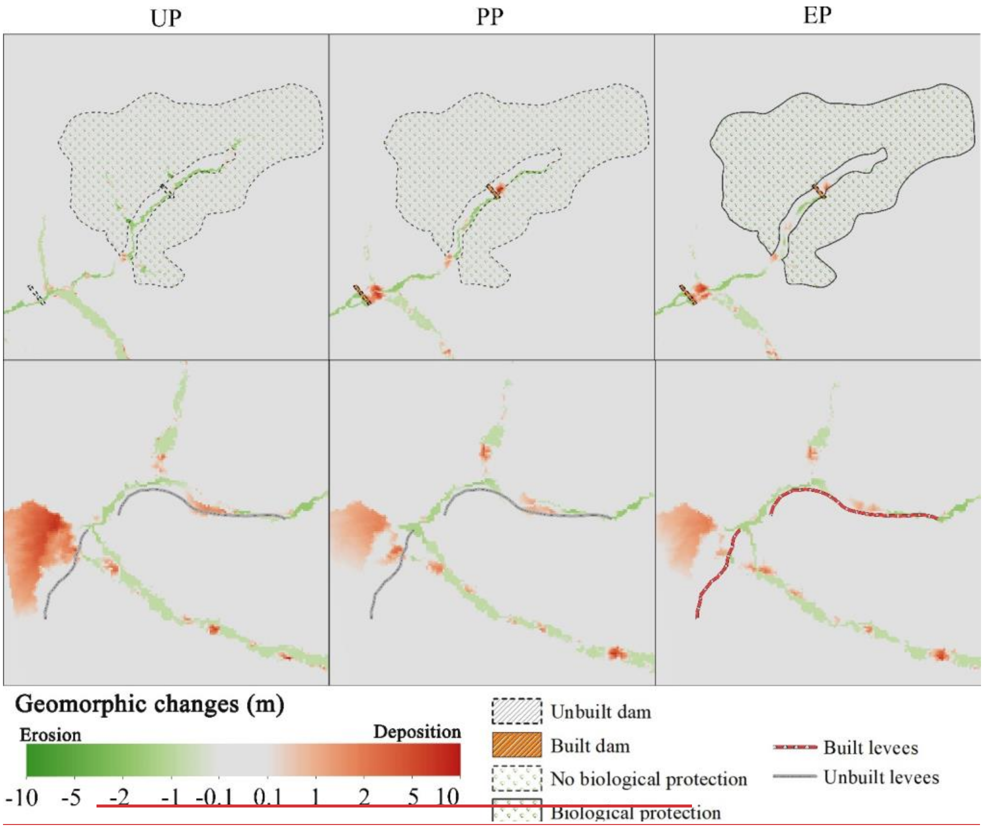

Figure 9: Geomorphic changes ~~in~~at the conclusion of the simulation at key spots ~~(the~~ for the UP, PP, and EP scenarios. The top row is the upriver section containing dam 1, dam 2 ~~in Scenario PP and EP~~ and the vegetation revetment ~~in Scenario EP showed in the first row;~~. The bottom row is the downriver section containing levees ~~in Scenario EP represent in the second row)~~.

带格式的: Captions, 左, 缩进: 左侧: 0 厘米, 右侧: 0 厘米, 段落间距段后: 0 磅, 行距: 单倍行距

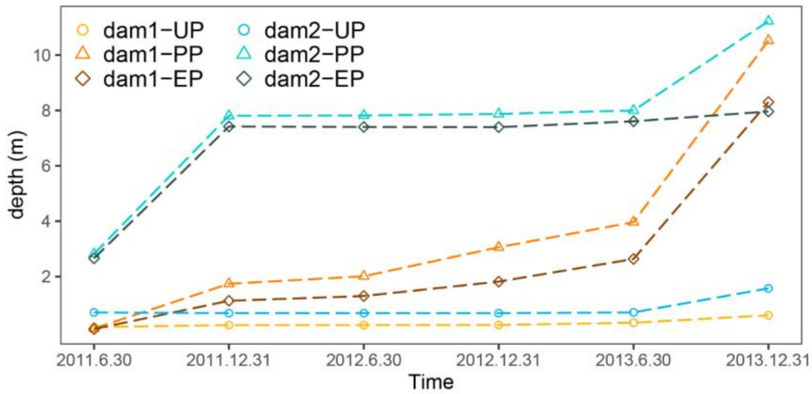

~~Fig. 7.~~

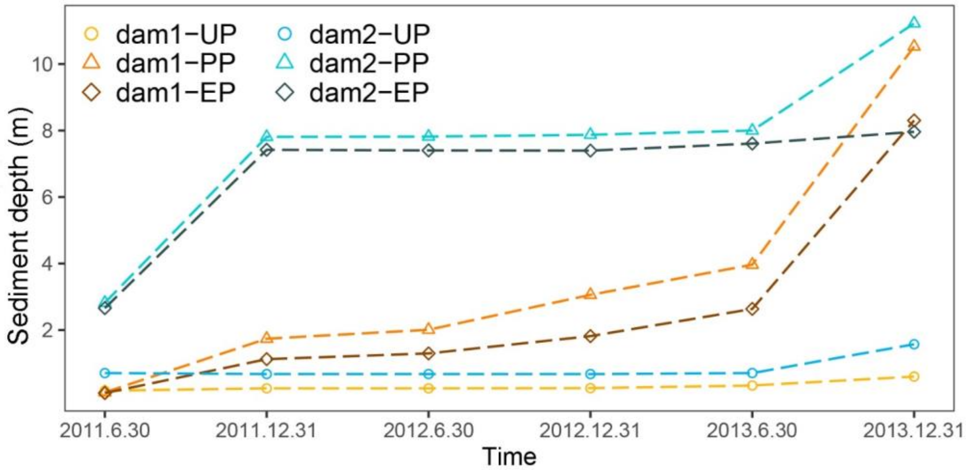

Figure 10: The depth of deposited sediment ~~blocked by dams in three scenarios~~in the dams' placements.

带格式的: Captions, 左, 缩进: 左侧: 0 厘米, 右侧: 0 厘米, 段落间距段后: 0 磅, 行距: 单倍行距

~~4. 3 Divisional erosion and deposition~~

~~We analyzed the source area, translation area, and deposit area by calculating the eroded and accumulated sediment volume. Fig. 8 shows the erosion and deposition distribution induced by rain over three years. The data showed similar phenomena in three scenarios, i.e., the eroded volume in the source area was less than that in the deposit area, and both were less than that in the translation area. The degree of deposition in the source area was less than that in the translation area, and the largest deposition was in the deposit area.~~

~~From the analysis of sediment conservation ability (see section 3.3) in each region controlled by different measures in three scenarios, the deposit area was the best at all times, and the source area was the worst. Dam 1 in the source area and Dam 2 in the translation area were so effective that the materials conservation ability increased by 138.1% and 52.5% in Scenario PP compared with Scenario UP, respectively (Table 2). What's more, the mitigation measures with vegetation revetment and levees in Scenario EP worked better. The ability in the source area increased by 161.9%, and the levees helped increase by 3.49% compared with Scenario UP. Therefore, the dams were most effective in blocking sediment, the vegetation revetment strengthened the conservation ability, and the levees worked mainly to prevent damage.~~

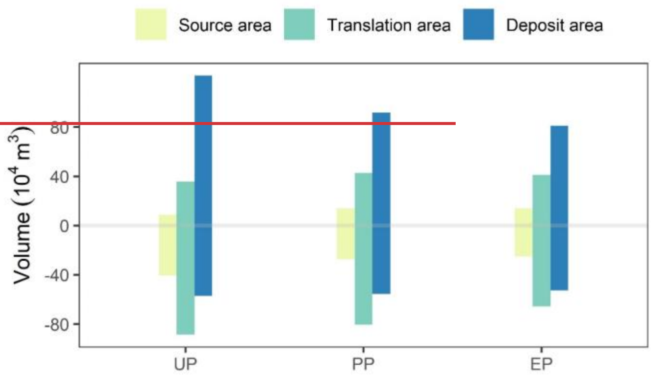

Fig. 8. The deposition and erosion volumes in different areas

Table 3 The sediment conservation ability

Region / Scenario	UP	PP	EP
Source area	0.21	0.50	0.55
Translation area	0.40	0.61	0.62
Deposit area	0.86	0.86	0.89

4.4 Effectiveness assessment

设置了格式：字体：Times New Roman，10 磅
带格式的：缩进：左侧： 0 厘米，行距：单倍行距
设置了格式：字体：Times New Roman

Fig. 9Figure 11 shows the erosion and deposition volumes in the source, transitional, and deposit areas and compares *Ca* in each scenario. The data showed similar phenomena in three scenarios. For example, the deposition volume in the source area was less than that in the transitional area, and the largest amount of sediment was deposited in the deposit area. Regarding the eroded sediment, the largest volume was in the transitional area, and the least was in the source area. Moreover, sediment transport could be controlled the best in the deposit area and the worst in the source area in any intervention conditions. By comparing the *Ca* of the source area in Scenario UP, the value was increased by 138.1% in Scenario PP, which was responsible for the dam1. And then dam 2 in the transitional area reduced sediment loss effectively reflected by the 52.5% increase in *Ca*. Furthermore, the mitigation measures in Scenario PP with vegetation revetment and levees in Scenario EP worked better. The conservation ability in the source area increased by 161.9%, and the levees helped increase by 3.49% in the deposit area. Therefore, the dams are most effective in blocking sediment. The vegetation revetments strengthen the conservation ability, while the levees are helpful but with a discernable impact on sediment conservation.

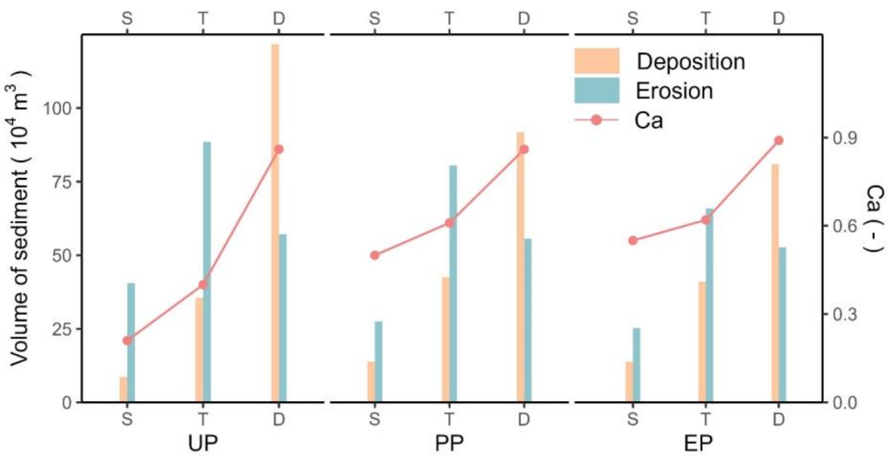

Figure 11: The volumes of sediment and the conservation ability (*Ca*) in three areas in each scenario (S: source area; T: transitional area; D: deposit area.).

Figure 12 presents the ~~time series of~~ cumulative sediment yield time series for each scenario ~~according to~~and the ~~output filer~~relative efficiency of scenario UP and EP. The steep curve of output cumulative sediment means ~~the great~~a significant increase of ~~sediment~~deposition, and three increasing stages have high consistency with the rainfall intensity in three monsoons (May-September). The total sediment output in UP was the largest, about 30.4×10^4 m^3, and the total ~~output~~production in PP (26.3×10^4 m^3) was larger than that in EP (19.3×10^4 m^3). ~~We used the formula mentioned in section 3.3 to calculate the~~

The relative efficiency over the period of controlling measures by human intervention in PP and EP ~~(Fig. 9b). Three~~(Figure 12b) indicates three distinct stages ~~were clear for the effective degree between PP and EP. The stage~~. Stage I ~~showed~~shows that the ~~two dams~~intervention measures in ~~PP or two dams with two levees and vegetation protection in EP~~ both ~~controlled~~scenarios prevented the sediment ~~loss~~transport completely. Later stage II ~~was an existing and~~ is a peculiar period ~~where~~when the effect of enhanced protective measures in EP was not as good as that in PP ~~after many simulation trials.~~through repeated experiments, which the increasing complexity of the model would cause. In stage III, the relative efficiency of the intervention measures in EP was greater than that in UP, which could achieve long-term ~~effective~~effect and stable conservation of solid materials. ~~What's more, the relative efficiency values in PP's stage III showed a decreasing trend, whereas the values declined indeterminately in EP's stage III because of the slight increase in values at the end of the simulation. In general, the engineering works in controlling sediment transport were efficient, and it would be better at protecting the fragile environment effectively with other intervention measures like vegetation revetment and levees. In addition, the effectiveness of conservation and mitigation would decrease with time.~~

带格式的：缩进：左侧： 0 厘米，首行缩进： 0 厘米，右侧： 0 厘米，行距：单倍行距

设置了格式：字体：Times New Roman

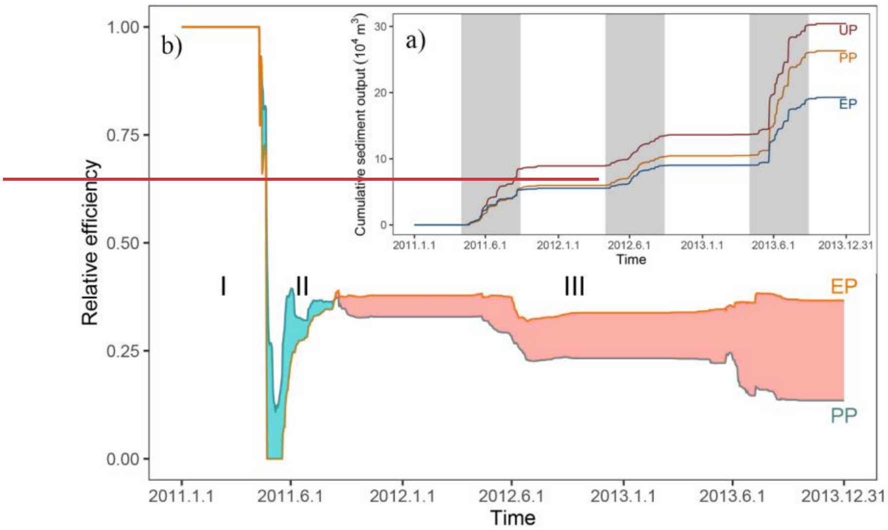

~~Fig. 9.~~

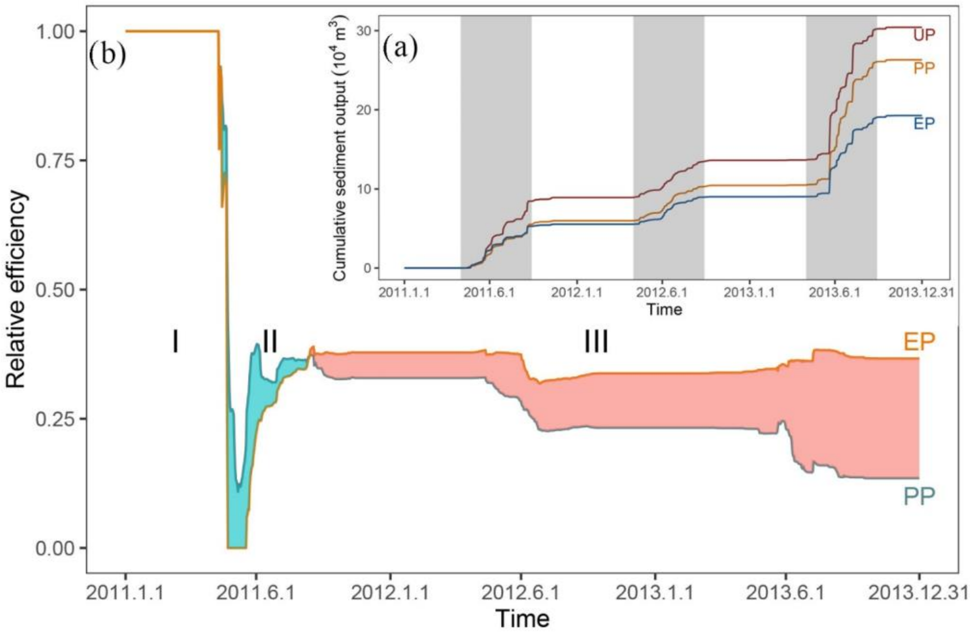

Figure 12: (a) showing the ~~output~~ cumulative output sediment over time (grey region highlighting three monsoons~~);~~), (b) showing the relative efficiency of scenario UP and EP compared with the UP (~~green region representing PP~~cyan shading represents when PP is more effective than EP and red ~~region standing~~shading represents the opposite)

带格式的: Captions, 左, 缩进: 左侧: 0 厘米, 右侧: 0 厘米, 段落间距段后: 0 磅, 行距: 单倍行距

5. Discussion

5.1 Model uncertainty and application

Reliability and uncertainty deserve a discussion for understanding and implementing the simulation results in most geographical analyses and modeling processes (Yeh and Li, 2006). Comparative simulation tests using the C-L tool suggested a complex spatial and temporal evolution of sediment transport. In addition, the tool demonstrated that the efficiency according to space and time varied in scenarios, which differed in control measures conducted on the mountainous areas that are susceptible to secondary geo-hazards. In this study, for the parameters involving geological conditions, we cited local research and comprehensive parameter sensitivity papers; we downscaled the daily rainfall sequence into hourly rainfall data collected in 2016 for every year because the total rainfall and intensity were identified as 'normal year' rainfall in 2016 (Xie et al., 2018). For the generated input data, although the intensity and event time would not be the same as the actual value, the realization of total rainfall in three different years suggested reasonable differences.

In addition, the optimal simulation result was decided according to the sediment depth in dam reservoirs and output between simulation and actual measurement from field survey or literature research. Fig. 10a shows the sediment distribution blocked by dam 1 in August 2012; the distance from the dam crest to the deposition level was up to 7 m, which suggested that the buried dam depth was nearly 3 m (dam height: 10 m). Therefore, the 3 m-depth simulation result of PP in the same moment found in Fig. 6 (see section 4.2) was consistent with the actual value. In October 2013, the same location collected by photo in Fig. 10b showed that the reservoir was full of materials, which were equal to the simulation depth of more than 10 m in Fig. 6. Conversely, the sediment yield in 2013 was up to 29.5×10^4 m^3 (Feng et al., 2017), which was from mainly the Shicouzi gully. Coincidentally but more scientifically, the apparent new erosion that occurred in 2013 in Shicouzi (Fig. 4) suggested the disaster history was rebuilt successfully by simulation, and the erosion volume in Shicouzi was 20.6×10^4 m^3. Therefore, it was reasonable that the simulation of eroded materials from Shicouzi accounted for 70% of the sediment from the left branch gully.

Fig. 10. The photos of dam 1 reservoir (the red single arrows showing the azimuth angle and the double arrows showing the height of the dam body)

设置了格式: 字体: Times New Roman, 加粗
带格式的: 缩进: 左侧: 0 厘米, 行距: 单倍行距
设置了格式: 字体: Times New Roman
设置了格式: 字体: Times New Roman, 10 磅
设置了格式: 字体: Times New Roman

Uncertainty deserves a discussion for understanding and implementing the simulation results in most geographical analyses and modelling processes (Yeh and Li, 2006). Comparative simulation tests using the C-L tool suggested a complex spatial and temporal evolution of sediment transport. They demonstrated that the efficiency varied in scenarios, which differed in control measures conducted on the mountainous areas susceptible to secondary geo-hazards. In this study, we cited local research and comprehensive parameter sensitivity papers for the parameters involving geological conditions. We downscaled the daily rainfall sequence into hourly data collected in 2016 for every year because the total rainfall and intensity were identified as a 'normal year' in 2016 (Xie et al., 2018). Although the intensity and event time would not be the same as the actual value for the generated input data, the realisation of total rainfall in three different years suggested reasonable differences.

The methods applied in the study further demonstrate the role of C-L as a tool to understand the short-medium term or long-term geomorphology changes (Ramirez et al., 2022; Li et al., 2020; Coulthard et al., 2012a) and observe the effectiveness of natural hazard interventions measures provided different rainfall patterns. For example, the mitigation facilities in this study were effective, especially engineering efforts cooperating with vegetation revetments in the upstream area, which would help decision-makers to optimise the management strategies to control mountain disasters. Geotechnical engineering has disadvantages, even though it is a mature technology that identifies and fixes problems quickly (Cui and Lin, 2013), such as the greater work and expense and the difficulty of maintenance. While the 'green development', the vegetation cover was effective in preventing erosion by strengthening topsoil and absorbing excess rainwater with its roots (Reichenbach et al., 2014; Stokes et al., 2014; Forbes and Broadhead, 2013; Mickovski et al., 2007). Alternatively, the methods could be used to study the tree planting patterns on different slopes.

5.2 Short-medium term problem

设置了格式: 字体: Times New Roman, 10 磅

带格式的: 行距: 单倍行距

设置了格式: 字体: Times New Roman

We used an ingenious and simple method to build the dams and levees in the simulation by increasing the elevation in the expected location and assuming that it could not be eroded (see ~~https://sourceforge.net/projects/caesar-~~ https://source~~lisflood/~~forge.net/projects/caesar~~). This method proved to be experimentally feasible (Gioia and Schiattarella, 2020; Poeppl et al., 2019). The rigid dam and levee body embedded in the model would not be broken, and the effect would not be weakening, so the result of geo-hazard risk assessment would be reduced to some extent. Although the fast and large amount of moving debris triggered a tremendous impact in the simulation, the tools could not simulate the geo-hazard chain links and would ignore the fierce attack on the environment and facilities downstream. Some typical geo-hazard chains were focused on the specified event in a short time and recreated the hazard lifecycle using physical and mechanical models (Fan et al., 2019). We concentrated on the effectiveness of mitigation measures in the short-medium term, which is different from those in space-time scales and purposes. Therefore, the three-year simulation time made it underestimated risk assessment, and a success to simulate the effect of mitigation measures compared with the actual result in this study.~~

~~5. 3 Sediment transport patterns~~

~~Different from~~lisflood/). This method proved to be experimentally feasible (Gioia and Schiattarella, 2020; Poeppel et al., 2019). The rigid dam and levee body embedded in the model would not be broken, and the effect would not weaken, so the result of the geo-hazard risk assessment would be reduced to some extent. Although the short and large number of moving debris triggered a tremendous impact in the simulation, the tools could not simulate the geo-hazard chain links. They would ignore the fierce attack on the environment and facilities downstream. Some typical geo-hazard chains were focused on the specified event in a short time and recreated the hazard lifecycle using physical and mechanical models (Fan et al., 2020). We concentrated on the effectiveness of mitigation measures in the short-medium term, which is different from those in space-time scales and purposes. Therefore, the three-year simulation time made it underestimated risk assessment and success to simulate the effect of mitigation measures compared with the actual result in this study.

5.3 Sediment transport patterns

Unlike the typical debris flow research, where three divided areas get their names for the materials process, the simulation result demonstrated that the loose solid materials from the source area sliding to the resting area were the least among the three regions, even for the scenario UP (unprotected landscapes). The sediment transport patterns change considerably~~ and two reasonable descriptions are as follows:~~. First, the abundant loose solid materials formed by the strong earthquake have ~~stabilized~~stabilised generally since ~~2008's~~2008's debris flow (details in Table ~~1~~S1). Second, the long~~,~~ and deep~~, and steep~~ gullies are mainly located in the ~~translation~~transitional area (Yaogouli, Shicouzi, Yangjiashan) and deposit area (Qinggangping~~). Thus, the large erodible area and the poor topographic conditions destroyed the circulation and deposit area~~), which provide more sediment supply than the source area. ~~Just as~~As shown in Fig. ~~11 shows~~S4, the movement of the materials occurred mainly in the branches in the ~~circulation~~transitional and deposit area. Moreover, the mitigation measures intervened in surface process, which lead to the changes in erosion and deposition in three areas. For example, an increase of deposition and a reducing of erosion appeared to be in source and transitional area, while the sediment deposition reduced significantly in deposit ~~area.~~ zone.

~~Fig. 11. Photos showing hazards sites in different areas: a) the source area, b) the deposit area, c) and d) the translation area~~

5.4 Long-term ~~trials~~ effectiveness

In the ~~future warmer world with more water vapor in the atmosphere, precipitation extremes will be intensified, increasing the likelihood of extreme and intense rainfall (East and Sankey, 2020). Then sequential increased fluvial transport capacity and erosion would accelerate geomorphic changes. With increased uncertainty of precipitation and temperature, future work about landscape evolution of three scenarios will help to understand long timescale effectiveness of intervention measures. We randomly selected one of the 50 repeat datasets downscaled by Li et al., (2020), which were generated in 2013-2025 and RCP 4.5 emission scenario from NEX-GDDP (spatial resolution: 0.25°×0.25°, temporal resolution: daily) to simulate the effectiveness in three scenarios. The result (Fig. 12) illustrated that stage III (stable stage started on the 161st day, in which Scenario EP's~~

带格式的：缩进：左侧：0 厘米，首行缩进：0 厘米，右侧：0 厘米，行距：单倍行距

设置了格式：字体：Times New Roman，10 磅

设置了格式：字体：Times New Roman

带格式的：缩进：左侧：0 厘米，行距：单倍行距

带格式的：缩进：左侧：0 厘米，首行缩进：0 厘米，右侧：0 厘米，行距：单倍行距

intervention measures were more effective) was more than stage I and II, which were only in the beginning. The relative effectiveness in both scenarios decreased gradually and the curve went down faster in PP than thatwarmer world, with more water vapour in the atmosphere, precipitation extremes will intensify, increasing the likelihood of extreme and intense rainfall (East and Sankey, 2020). Then sequential increased fluvial transport capacity and erosion would accelerate geomorphic changes. With increased uncertainty of precipitation and temperature, future work on the landscape evolution of three scenarios will help to understand the long-timescale effectiveness of intervention measures. We randomly selected one of the 50 repeat datasets downscaled by Li et al. (2020), which were generated in 2013-2025 and RCP 4.5 emission scenario from NEX-GDDP (spatial resolution: 0.25°×0.25°, temporal resolution: daily) to simulate the effectiveness in three scenarios. The result (Figure 13) illustrated that stage III (the stable stage that started on the 161st day, in which Scenario EP's intervention measures were more effective) was more than stages I and II, which were only in the beginning. The relative effectiveness in both scenarios decreased gradually, and the curve went down faster in PP than in EP.

We further explain the change in intervention effectiveness over time. The effectiveness of controlling sediment transport is primarily for two reasons. The first one concerns the sediment trapping capability of checking dams and the increase of soil's infiltration capacity with vegetation roots. Another is because of the positive feedback about the geomorphic changes, especially the deposition behind the dams. Because the gradient of the upriver channel is slowed down by checking dams, and the sediment carry capacity from the flow is reduced (Luan et al., 2022; Hassanli and Beecham, 2013). The storage capacity of checking dams fades as the accumulation of sediment deposits, which necessarily lead to the gradual decrease of intervention effectiveness. Additionally, the vegetation revetments still reduce sediment transport by stabilising topsoil over the period when the reservoirs are filling with sediment without dredging work. Therefore, the effectiveness of compound measures in Scenario EP goes down with a gentler downward trend.

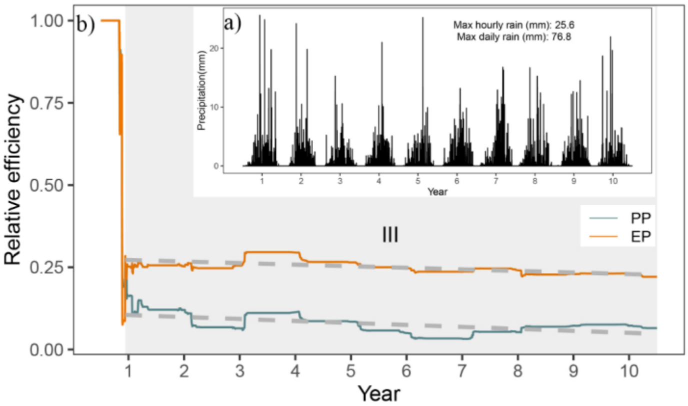

Fig. 12. a) RainfallFigure 13: (a) rainfall downscaled from stochastic future rainfall; (b) the relative efficiency changes over ten years (grey region highlighting stage III, and the grey dashed lines indicated the linear fitting curve)

6. Conclusions

In this study, we compared the scenarios intervented by check dams, biological measures and artificial barriers using the C-L model to outline the affected area, measure the impacts of blocking sediment, and examine how the vegetable revetments helped to stabilise the slope. We have four key findings. First, the comparative scenario simulations showed that mitigation measures in scenario PP (containing two blocking dams) and scenario EP (incorporating biological processing in the

设置了格式：字体：10 磅

带格式的：图片表格，左，右侧： 0 厘米，行距：单倍行距，与下段同页

设置了格式：字体：Times New Roman，加粗

带格式的：缩进：左侧： 0 厘米，段落间距段后：0 磅，行距：单倍行距

设置了格式：字体：Times New Roman

设置了格式：字体颜色：自动设置

source area with two dams) were effective in reducing erosion, engineering works in controlling sediment output, and protecting property from damage in post-earthquake fragile mountains prone to secondary geo-hazards. Erosion had a high consistency with the monsoons (May-September)transport are efficient, and was mainly in the upper reaches and the left branches of the main gully. The two dams have blocked the upstream sediment successfully and the levees had an important role in preventing the debris shocking, and burial of the residents and cultivated land along the river. In addition, the decrement in EP suggested the accumulated materials blocked by dams upgrade a slope upstream in turn. What's more, model embedded quantification ofit would be better at protecting the fragile environment effectively with other intervention measures like vegetation revetment showed that the sediment yielded decreased 5 times as much as scenario UP, which contributed to that the vegetation cover enhanced precipitation infiltration and reduced flow velocity.

and artificial barries. Second, reasonable and comprehensive treatment methods for a mountainous area with abundant solid materials reduced internal geomorphology changes and sediment output. The areas of erosion and deposition varied in degree decreased in EP compared with PP, except for heavy deposition. Then both the internal damaged area and the erosion volume in EP were less than in PP. In addition, the reduced volume of erosion in the source area between EP and PP was larger than the deposition volume suggesting the vegetation protection was effective in EP. Conversely, three years later, the simulated depth of accumulation blocked by dam 1 and dam 2 was greater than the height of the dams in PP, whereas only the depth deposited in the upriver of dam 2 was greater than the dam height. Moreover, the present intervention measures are not adequate to reduce erosion and should be combined with dredging work.

Third, zonal statistics of the volumes of erosion and deposition in the source area, translation area, and deposit area demonstrated thatthe effectiveness of conservation and mitigation would decrease over time. Third, the characteristics of sediment transport patterns changed considerably. The conservation ability in the deposit area was the best at all times, and the source area was the worst. Dam 1 in the source area and dam 2 in the translation area worked so well that the materials conservation ability increased by 138.1% and 52.5% compared with the scenario without any by the intervention method. With the extra help of vegetation revetment, the measures. The stabilising sediment ability in the source area increased by 161.9%, and the levees helped the deposit area increase by 3.49%. % with the additional help of vegetation revetments. At last, the present intervention measures are inadequate to reduce erosion and should be combined with dredging work.

Fourth, the two types of effectiveness found in the sediment output simulated under Scenario PP and EP compared with Scenario UP were divided into three apparent stages with a general downward trend. The first stage was completely effective in both PP and EP, whereas stage Ⅱ was a peculiar period in which the effect in EP was not as good as that in PP, which would be caused by the increasing complexity of the model. Lastly, steady effectiveness would be sustainable as shown in stage Ⅲ, in which the effectiveness simulated in EP with vegetation revetment and levees was greater than that in PP.

Taking long-term effectiveness and the function of vegetation into consideration for mitigation measures is more helpful to understand the efficiency. More works should be carried out to explore, especially with the increased likelihood of extreme and intense rainfall in the future.

设置了格式：字体颜色：自动设置

设置了格式：字体颜色：自动设置

设置了格式：字体颜色：自动设置

设置了格式：字体颜色：自动设置

带格式的：缩进：左侧： 0 厘米，首行缩进： 0 厘米，右侧： 0 厘米，行距：单倍行距

设置了格式：字体颜色：自动设置

设置了格式：字体颜色：自动设置

设置了格式：字体颜色：自动设置

设置了格式：字体颜色：自动设置

Declaration of interest statement

The authors declare that they have no known competing financial interests or personal relationships that could have appeared to influence the work reported in this paper.

Author contribution

Di Wang: ~~Conceptualization~~Conceptualisation, Methodology, Software, Writing-original draft preparation. Ming Wang and Kai Liu: Supervision, Methodology, Writing- Reviewing and Editing, Validation.

Acknowledgments

This research was supported by the National Key Research and Development Plan (2017YFC1502902). The financial support is highly appreciated. The authors would also like to thank Professor Tom Coulthard and his team for their excellent work on the freely available C-L model (https://sourceforge.net/projects/ caesar-lisflood).

带格式的：缩进：左侧： 0 厘米，段落间距段后：0 磅，行距：单倍行距

带格式的：缩进：首行缩进： 0 厘米，段落间距段后：0 磅

带格式的：缩进：左侧： 0 厘米，段落间距段后：0 磅，行距：单倍行距

带格式的：段落间距段后：0 磅

带格式的：缩进：左侧： 0 厘米，段落间距段后：0 磅，行距：单倍行距

带格式的：缩进：左侧： 0 厘米，首行缩进： 0 厘米，右侧： 0 厘米，行距：单倍行距

Reference

带格式的：缩进：左侧： 0 厘米，段落间距段后：0 磅，行距：单倍行距

Arcement, G. J., and Schneider, V. R.: Guide for selecting Manning's roughness coefficients for natural channels and flood plains, United States Geological Survey Water-Suply Paper 2339, https://doi.org/https://doi.org/10.3133/wsp2339, 1989.

Bates, P. D., Horritt, M. S., and Fewtrell, T. J.,.: A simple inertial formulation of the shallow water equations for efficient two-dimensional flood inundation modelling, J. Hydrol., 387(1–2),, 33–45, https://doi.org/10.1016/j.jhydrol.2010.03.027, 2010.

Batty, M., Couclelis, H., and Eichen, M.: Urban systems as cellular automata, Environ Plan B Urban Anal City Sci, 24(2), 159–305, https://doi.org/10.1068/b240159, 1997.

Batty, M.,. and Xie, Y.: Possible urban automata, Environ Plann. Plan. B PlannPlan. Des,., 24(2),, 175–192,, https://doi.org/10.1068/b240175, 1997.

Beven, K.: LINKING PARAMETERS ACROSS SCALES : SUBGRID PARAMETERISATIONS AND SCALE DEPENDENT HYDROLOGICAL MODELS, Hydrol. Process., 9, 507–525, https://doi.org/https://doi.org/10.1002/hyp.3360090504, 1995.

Beven, K.: TOPMODEL : A CRITIQUE, Hydrol. Process., 11, 1069–1085, https://doi.org/https://doi.org/10.1002/(SICI)1099-1085(199707)11:9<1069::AID-HYP545>3.0.CO;2-O, 1997.

Beven, K. J.,. and Kirkby, M. J.: A physically based, variable contributing area model of basin hydrology, Hydrol. Sci J.,. Bull., 24(1),, 43–69, https://doi.org/10.1080/02626667909491834, 1979.

Chen, N., Zhou, H., Lu, YYang, L., Yang, L., and Lv, L.: Analysis of benefits of debris flow control projects in southwest mountains areas of China (In Chinese). Journal of, J. Chengdu University of TechnologyUniv. Technol. (Science and Technology Edition),Technol. Ed., 40(1),, 50–58, https://doi.org/10.3969/j.issn.1671-9727.2013.01.008, 2013.

Chen, X., Li, Z., Cui, P., and Liu, X.: Estimation of soil erosion caused by the 5.12 Wenchuan Earthquake, J. Mt. Sci., 27, 122–127, 2009.

Cong, K., Li, R., and Bi, Y.: Benefit evaluation of debris flow control engineering based on the FLO-2D model (In Chinese), Northwestern Geology, 52(3),, Northwest. Geol., 52, https://doi.org/10.19751/j.cnki.61-1149/p.2019.03.019, 2019.

Couclelis, H.: From cellular automata to urban models: new principles for model development and implementation, Environ Plann. Plan. B PlannPlan. Des,., 24(2),, 165–174, https://doi.org/10.1068/b240165, 1997.

Coulthard, T J,Coulthard, T. J. and Skinner, C. J.: The sensitivity of landscape evolution models to spatial and temporal rainfall resolution, Earth Surf. Dyn., 4, 757–771, https://doi.org/10.5194/esurf-4-757-2016, 2016.

Coulthard, T. J. and Van De Wiel, M. J.: Modelling long term basin scale sediment connectivity, driven by spatial land use changes, Geomorphology, 277, 265–281, https://doi.org/10.1016/j.geomorph.2016.05.027, 2017.

Coulthard, T. J., Macklin, M. G., and Kirkby, M. J.: A cellular model of Holocene upland river basin and alluvial fan evolution, Earth Surf. Process Landf. Landforms, 27(3),, 269–288, https://doi.org/10.1002/esp.318, 2002.

Coulthard, TomT. J., Hancock, G. R., and Lowry, J. B. C.: Modelling soil erosion with a downscaled landscape evolution model, Earth Surf. Process Landf. Landforms, 37(10),, 1046–1055, https://doi.org/10.1002/esp.3226, 20122012a.

Coulthard, Tom J,Coulthard, T. J., Ramirez, J., Fowler, H. J., and Glenis, V.: Using the UKCP09 probabilistic scenarios to model the amplified impact of climate change on drainage basin sediment yield, Hydrol. Earth Syst. Sci., 16, 4401–4416, https://doi.org/10.5194/hess-16-4401-2012, 2012b.

Coulthard, T. J., Neal, J. C., Bates, P. D., Ramirez, J., de Almeida, G. A. M., and Hancock, G. R.: Integrating the LISFLOOD-FP 2D hydrodynamic model with the CAESAR model: Implications for modelling landscape evolution, Earth Surf. Process Landf. Landforms, 38(15),, 1897–1906, https://doi.org/10.1002/esp.3478, 2013.

设置了格式

带格式的：缩进：左侧： 0 厘米，首行缩进： 0 厘米，行距：单倍行距

带格式的：缩进：左侧： 0 厘米，首行缩进： 0 厘米，行距：单倍行距

带格式的：缩进：左侧： 0 厘米，首行缩进： 0 厘米，行距：单倍行距

带格式的：缩进：左侧： 0 厘米，首行缩进： 0 厘米，行距：单倍行距

带格式的：缩进：左侧： 0 厘米，首行缩进： 0 厘米，行距：单倍行距

带格式的：缩进：左侧： 0 厘米，首行缩进： 0 厘米，行距：单倍行距

Cui, P. and Lin, Y.: Debris-Flow Treatment: The Integration of Botanical and Geotechnical Methods, J. Resour. Ecol., 4, 097–104, https://doi.org/10.5814/j.issn.1674-764x.2013.02.001, 2013.

Cui, P., Zhou, G. G. D., Zhu, X. H., and Zhang, J. Q.: Scale amplification of natural debris flows caused by cascading landslide dam failures., Geomorphology (Amst) , 182(August 2010),, 173–189, https://doi.org/10.1016/j.geomorph.2012.11.009, 2013.

带格式的: 缩进: 左侧: 0 厘米, 首行缩进: 0 厘米, 行距: 单倍行距

East, A. E.,, and Sankey, J. B.: Geomorphic and Sedimentary Effects of Modern Climate Change: Current and Anticipated Future Conditions in the Western United States., Rev. Geophys., 58(4), , https://doi.org/10.1029/2019RG000692, 2020.

Einstein, H. A.: The Bed-Load Function for Sediment Transportation in Open Channel Flows, 1950.

Fan, X., Yang, F., Siva Subramanian, S., Xu, Q., Feng, Z., Mavrouli, O., Peng, M., Ouyang, C., Jansen, J. D., and Huang, R.: Prediction of a multi-hazard chain by an integrated numerical simulation approach: the Baige landslide, Jinsha River, China, Landslides, 17(1),, 147–164, https://doi.org/10.1007/s10346-019-01313-5, 20192020.

带格式的: 缩进: 左侧: 0 厘米, 首行缩进: 0 厘米, 行距: 单倍行距

Feng, W., He, S., Liu, Z., Yi, X., and Bai, H.: Features of debris flowsDebris Flows and their engineering control effects at xinping gully of pingwu county (In Chinese) , Journal of Their Engineering Geology,Control Effects at Xinping Gully of Pingwu County, J. Eng. Geol., 25(3), 794–805, https://doi.org/10.13544/j.cnki.jeg., 2017.03.027, 2017.

Forbes, K. and Broadhead, J.: Forests and landslides: the role of trees and forests in the prevention of landslides and rehabilitation of landslide-affected areas in Asia, FAO, 14–18 pp., 2013.

Gioia, D.,, and Schiattarella, M.: Modeling Short-Term Landscape Modification and Sedimentary Budget Induced by Dam Removal: Insights from LEM Application, Appl. Sci., 10, 7697, https://doi.org/10.3390/app10217697, 2020.

带格式的: 缩进: 左侧: 0 厘米, 首行缩进: 0 厘米, 行距: 单倍行距

Goldberg, D. E.,: Genetic Algorithms in Search, OptimizationOptimisation, and Machine Learning, 35, 2, Addison-Wesley Longman Publishing Co., Inc,., 372 pp., https://doi.org/10.1007/BF01920603, 1989.

Gorum, T., Fan, X., van Westen, C. J., Huang, R. Q., Xu, Q., Tang, C., and Wang, G.: Distribution pattern of earthquake-induced landslides triggered by the May 12 2008 Wenchuan earthquake, Geomorphology, 133, 152–167, https://doi.org/10.1016/j.geomorph.2010.12.030, 2011.

Guo, Q., Xiao, J., and Guan, X.: The characteristics of debris flow activities and its optimal timing for the control in Shikan River Basin Pingwu Country (In, Chinese), The Chinese Journal of Geological J. Geol. Hazard and Control, 29(115(03)), 37–43, https://doi.org/10.16031/j.cnki.issn.1003-8035.2018.03.05, 2018.

带格式的: 缩进: 左侧: 0 厘米, 首行缩进: 0 厘米, 行距: 单倍行距

Hancock, G. R., Verdon-Kidd, D., and Lowry, J. B. C.: Soil erosion predictions from a landscape evolution model – An assessment of a post-mining landform using spatial climate change analogues, Sci. Total Environ,., 601–602, 109–121, https://doi.org/10.1016/j.scitotenv.2017.04.038, 2017.

Highland, LHassanli, A. M.,, and Bobrowsky, P.: The landslide Handbook - A guide to understanding landslides, In US Geological Survey Circular, 1325, Beecham, S.: Criteria for optimising check dam location and maintenance requirements, Check Dams, Morphol. Adjust. Eros. Control Torrential Streams, 11–31, 2013.

He, J., Zhang, L., Fan, R., Zhou, S., Luo, H., and Peng, D.: Evaluating effectiveness of mitigation measures for large debris flows in Wenchuan, China, Landslides, 19, 913–928, https://doi.org/10.3133/cir1325, 20081007/s10346-021-01809-z, 2022.

带格式的: 缩进: 左侧: 0 厘米, 首行缩进: 0 厘米, 行距: 单倍行距

Huang, R.,: Geohazard assessment of the Wenchuan earthquake (In Chinese),, Science Press, Beijing, 944 pp., 2009.

Huang, R. and Fan, X.: The landslide story, Nat. Geosci., 6, 325–326, https://doi.org/10.1038/ngeo1806, 2013.

J.B.C.Lowry, M.Narayan, G.R.Hancock, K.G.Evans, and K.G.Evans.,: Understanding post-mining landforms: Utilising pre-mine geomorphology to improve rehabilitation outcomes, Geomorphology (Amst),, 328, 93–107, https://doi.org/10.1016/j.geomorph.2018.11.027, 2019.

带格式的: 缩进: 左侧: 0 厘米, 首行缩进: 0 厘米, 行距: 单倍行距

Lan, H., Wang, D., He, S., Fang, Y., Chen, W., Zhao, P., and Qi, Y.: Experimental study on the effects of tree planting on slope stability, Landslides, 17, 1021–1035, https://doi.org/10.1007/s10346-020-01348-z, 2020.

Lee, T.,, and Jeong, C.: Nonparametric statistical temporal downscaling of daily precipitation to hourly precipitation and implications for climate change scenarios, J. Hydrol., 510, 182–196, https://doi.org/10.1016/j.jhydrol.2013.12.027, 2014.

带格式的: 缩进: 左侧: 0 厘米, 首行缩进: 0 厘米, 行距: 单倍行距

Li, C., Wang, M., and Liu, K.: A decadal evolution of landslides and debris flows after the Wenchuan earthquake, Geomorphology (Amst),, 323, 1–12, https://doi.org/10.1016/j.geomorph.2018.09.010, 2018.

Li, C., Wang, M., Liu, K., and Coulthard, T. J.,.: Landscape evolution of the Wenchuan earthquake-stricken area in response to future climate change, J J. Hydrol., 590(June),, 125244, https://doi.org/10.1016/j.jhydrol.2020.125244, 2020.

Luan, J., Miao, P., Tian, X., Li, X., Ma, N., Xu, Z., Wang, H., and Zhang, Y.: Separating the impact of check dams on runoff from climate and vegetation changes, J. Hydrol., 614, 128565, https://doi.org/10.1016/j.jhydrol.2022.128565, 2022.

Marchi, L., Comiti, F., Crema, S., and Cavalli, M.: Channel control works and sediment connectivity in the European Alps, Sci. Total Environ., 668, 389–399, https://doi.org/10.1016/j.scitotenv.2019.02.416, 2019.

Mickovski, S. B., Bengough, A. G., Bransby, M. F., Davies, M. C. R., Hallett, P. D., and Sonnenberg, R.: Material stiffness, branching pattern and soil matric potential affect the pullout resistance of model root systems, Eur. J. Soil Sci., 58, 1471–1481, https://doi.org/10.1111/j.1365-2389.2007.00953.x, 2007.

Poeppl, R. E., Coulthard, T., Keesstra, S. D., and Keiler, M.: Modeling the impact of dam removal on channel evolution and sediment delivery in a multiple dam setting, Int. J. Sediment Res,., 34(6),, 537–549, https://doi.org/10.1016/j.ijsrc.2019.06.001, 2019.

Ramirez, J. A., Zischg, A. P., Schürmann, S., Zimmermann, M., Weingartner, R., Coulthard, T., and Keiler, M.: Modeling the geomorphic response to early river engineering works using CAESAR-Lisflood, Anthropocene, 32, https://doi.org/10.1016/j.ancene.2020.100266, 2020.

Ramirez, J. A., Mertin, M., Peleg, N., Horton, P., Skinner, C., Zimmermann, M., and Keiler, M.: Modelling the long-term geomorphic response to check dam failures in an alpine channel with CAESAR-Lisflood, Int. J. Sediment Res., 37, 687–700, https://doi.org/10.1016/j.ijsrc.2022.04.005, 2022.

Reichenbach, P., Busca, C., Mondini, A. C., and Rossi, M.: The Influence of Land Use Change on Landslide Susceptibility Zonation: The Briga Catchment Test Site (Messina, Italy), Environ. Manage., 54, 1372–1384, https://doi.org/10.1007/s00267-014-0357-0, 2014.

Saynor, M. J., Lowry, J. B. C., and Boyden, J. M.: Assessment of rip lines using CAESAR-Lisflood on a trial landform at the Ranger Uranium Mine, L Land. Degrad. Dev,., 30(5),, 504–514, https://doi.org/10.1002/ldr.3242, 2019.

Skinner, C. J., Coulthard, T. J., Schwanghart, W., Van De Wiel, M. J., and Hancock, G.,.: Global sensitivity analysis of parameter uncertainty in landscape evolution models, Geosci. Model Dev,., 11(12),, 4873–4888, https://doi.org/https://doi.org/10.5194/gmd-11-4873-2018, 2018.

Slingerland, N., Beier, N., and Wilson, G.: Stress testing geomorphic and traditional tailings dam designs for closure using a landscape evolution model, in: Proceedings of the 13th International Conference on Mine Closure, 1533–1544, https://doi.org/10.36487/ACG_rep/1915_120_Slingerland, 2019.

Stokes, A., Douglas, G. B., Fourcaud, T., Giadrossich, F., Gillies, C., Hubble, T., Kim, J. H., Loades, K. W., Mao, Z., McIvor, I. R., Mickovski, S. B., Mitchell, S., Osman, N., Phillips, C., Poesen, J., Polster, D., Preti, F., Raymond, P., Rey, F., Schwarz, M., and Walker, L. R.: Ecological mitigation of hillslope instability: Ten key issues facing researchers and practitioners, Plant Soil, 377, 1–23, https://doi.org/10.1007/s11104-014-2044-6, 2014.

Thomson, H.,. and Chandler, L.: Tailings storage facility landform evolution modelling, in: Proceedings of the 13th International Conference on Mine Closure, 385–396, https://doi.org/10.36487/ACG_rep/1915_31_Thomson, 2019.

Wang, M., Yang, W., Shi, P., Xu, C., and Liu, L.: Diagnosis of vegetation recovery in mountainous regions after the wenchuan earthquake, IEEE J. Sel. Top. Appl. Earth Obs. Remote Sens., 7, 3029–3037, https://doi.org/10.1109/JSTARS.2014.2327794, 2014a.

Wang, M., Liu, M., Yang, S., and Shi, P.: Incorporating Triggering and Environmental Factors in the Analysis of Earthquake-Induced Landslide Hazards, Int. J. Disaster Risk Sci., 5, 125–135, https://doi.org/10.1007/s13753-014-0020-7, 2014b.

带格式的：缩进：左侧： 0 厘米，首行缩进： 0 厘米，行距：单倍行距

带格式的：缩进：左侧： 0 厘米，首行缩进： 0 厘米，行距：单倍行距

带格式的：缩进：左侧： 0 厘米，首行缩进： 0 厘米，行距：单倍行距

Wang, N., Han, B., Pang, Q., and Yu, Z.: post-evaluation model on effectiveness of debris flow control, J. Eng. Geol., 23, 219–226, https://doi.org/10.13544/j.cnki.jeg.2015.02.005, 2015.

Van De Wiel, M. J., Coulthard, T. J., Macklin, M. G., and Lewin, J.: Embedding reach-scale fluvial dynamics within the CAESAR cellular automaton landscape evolution model, Geomorphology~~ (Amst)~~, 90~~(3)~~, 283–301, https://doi.org/10.1016/j.geomorph.2006.10.024, 2007.

Wilcock, P. R., Asce, M., and Crowe, J. C.: Surface-based Transport Model for Mixed-Size Sediment Surface-based Transport Model for Mixed-Size Sediment, 9429, https://doi.org/10.1061/(ASCE)0733-9429(2003)129, 2003.

~~Wang, M., Liu, M., Yang, S., and Shi, P.: Incorporating Triggering and Environmental Factors in the Analysis of Earthquake-Induced Landslide Hazards, Int. J. Disaster Risk Sci., 5(2), 125–135, https://doi.org/10.1007/s13753-014-0020-7, 2014.~~

~~Wang, M., Yang, W., Shi, P., Xu, C., and Liu, L.: Diagnosis of vegetation recovery in mountainous regions after the wenchuan earthquake, I IEEE J Sel Top Appl Earth Obs Remote Sens, 7(7), 3029–3037, https://doi.org/10.1109/JSTARS.2014.2327794, 2014.~~

~~Wang, N., Han, B., Pang, Q., and Yu, Z.: Post-evaluation model on effectiveness of debris flow control (In Chinese). Journal of Engineering Geology, 23(2), 219–226, https://doi.org/10.13544/j.cnki.jeg.2015.02.005, 2015.~~

Xie, J., Wang, M., Liu, K., and Coulthard, T. J.: Modeling sediment movement and channel response to rainfall variability after a major earthquake, Geomorphology~~ (Amst)~~, 320, 18–32, https://doi.org/10.1016/j.geomorph.2018.07.022, 2018.

Xu, C., Xu, X., Yao, X., and Dai, F.: Three (nearly) complete inventories of landslides triggered by the May 12, 2008 Wenchuan Mw 7.9 earthquake of China and their spatial distribution statistical analysis, Landslides, 11, 441–461, https://doi.org/10.1007/s10346-013-0404-6, 2014.

Yang, Z., Duan, X., Huang, J., Dong, Y., Zhang, X., Liu, J., and Yang, C.: Tracking long-term cascade check dam siltation: implications for debris flow control and landslide stability, Landslides, 18, 3923–3935, https://doi.org/10.1007/s10346-021-01755-w, 2021.

Yeh, A. G. O~~.,~~. and Li, X.: Errors and uncertainties in urban cellular automata, Comput. Environ. Urban Syst~~.,~~., 30~~(1)~~, 10–28, https://doi.org/10.1016/j.compenvurbsys.2004.05.007, 2006.

Yu, B., Yang, Y., Su, Y., Huang, W., and Wang, G.: Research on the giant debris flow hazards in Zhouqu County, Gansu Province on August 7, 2010~~ (In Chinese), Journal of Engineering Geology, 18(4),~~, J. Eng. Geol., 18, 437–444, https://doi.org/10.3969/j.issn.1004-9665.2010.04.001, 2010.

Zhang, L~~.,~~. and Liang, K.: Research on economic benefit evaluation of the prevention and cure project for debris flow~~ (In Chinese), The Chinese Journal of Geological~~ J. Geol. Hazard ~~and~~ Control, 16~~(3)~~, 48–53, https://doi.org/10.3969/j.issn.1003-8035.2005.03.011, 2005.

Zhang, X., Wang, M., Liu, K., Xie, J., and Xu, H.: Using NDVI time series to diagnose vegetation recovery after major earthquake based on dynamic time warping and lower bound distance, Ecol. Indic., 94~~(June)~~, 52–61, https://doi.org/10.1016/j.ecolind.2018.06.026, 2018.

~~Zhao, C., Liang, J., Xie, Z., She, T., and Zhang, S.: Remote sensing dynamic analysis of debris flow activity characteristics in strong earthquake area of Wenchuan earthquake 10 years after earthquake-A case study of shikan river watershed of pingwu county (In Chinese), Journal of Catastrophology, 34(4), 222–227, https://doi.org/10.3969/j.issn.1000-811X.2019.04.038, 2019.~~

带格式的：缩进：左侧： 0 厘米，首行缩进： 0 厘米，行距：单倍行距

带格式的：缩进：左侧： 0 厘米，首行缩进： 0 厘米，行距：单倍行距

带格式的：缩进：左侧： 0 厘米，首行缩进： 0 厘米，行距：单倍行距

Zhou, H., Chen, N., Lu, Y., and Li, B.: Control Effectiveness of Check Dams in Debris Flow Gully: A Case of Huashiban Gully in Earthquake Worst-stricken Area, , Beichuan County (In Chinese), Journal of Mountain Science,, J. Mt. Sci., 30(3),, 347–354, (https://doi.org/10.3969/j.issn.1008-2786.2012.03.015, 2012.

带格式的：缩进：左侧： 0 厘米，首行缩进： 0 厘米，行距：单倍行距

带格式的：行距：单倍行距